Geophys. J. Int. (2001) **144,** 577–596

Preliminary determination of the interdependence among strong-motion amplitude, earthquake magnitude and hypocentral distance for the Himalayan region

Imtiyaz A. Parvez,[1,3,*] Alexander A. Gusev,[2] Giuliano F. Panza[1,3] and Anatoly G. Petukhin[4]

[1] *Department of Earth Sciences, University of Trieste, Via E. Weiss* 4, 34127 *Trieste, Italy. E-mails: parvez@dst.univ.trieste.it; panza@dst.univ.trieste.it*
[2] *Institute of Volcanic Geology and Geochemistry, Russian Academy of Science,* 9 *Piip Boulevard, Petropavlovsk-Kamchatsky,* 683006, *Russia. E-mail: gusev@emsd.iks.ru*
[3] *The Abdus Salam International Centre for Theoretical Physics, SAND Group, Trieste, Italy*
[4] *Kamchatka Experimental and Methodical Seismological Department GS RAS* 9 *Piip Boulevard, Petropavlovsk-Kamchatsky,* 683006, *Russia. E-mail: petuhin@mail.ru*

Accepted 2000 September 19. Received 2000 July 26; in original form 2000 February 6

SUMMARY

Since the installation of three limited-aperture strong-motion networks in the Himalayan region in 1986, six earthquakes with $M_w = 5.2$–7.2 have been recorded up to 1991. The data set of horizontal peak accelerations and velocities consists of 182-component data for the hypocentral distance range 10–400 km. This data set is limited in volume and coverage and, worst of all, it is highly inhomogeneous. Thus, we could not determine regional trends for amplitudes by means of the traditional approach of empirical multiple regression. Instead, we perform the reduction of the observations to a fixed distance and magnitude using independently defined distance and magnitude trends. To determine an appropriate magnitude-dependent distance attenuation law, we use the spectral energy propagation/random function approach of Gusev (1983) and adjust its parameters based on the residual variance. In doing so we confirm the known, rather gradual mode of decay of amplitudes with distance in the Himalayas; this seems to be caused by the combination of high Qs and crustal waveguide effects for high frequencies. The data are then reduced with respect to magnitude. The trend of peak acceleration versus magnitude cannot be determined from observations, and we assume that it coincides with that of abundant Japanese data. For the resulting set of reduced $\log_{10}$ (peak acceleration) data, the residual variance is 0.37^2, much above commonly found values. However, dividing the data into two geographical groups, western with two events and eastern with four events, reduces the residual variance to a more usual level of 0.27^2 (a station/site component of 0.22^2 and an event component of 0.16^2). This kind of data description is considered acceptable. A similar analysis is performed with velocity data, and again we have to split the data into two subregional groups. With our theoretically grounded attenuation laws we attempt a tentative extrapolation of our results to small distances and large magnitudes. Our minimum estimates of peak acceleration for the epicentral zone of $M_w = 7.5$–8.5 events is $A_{peak} = 0.25$–0.4 g for the western Himalayas, and as large as $A_{peak} = 1$–1.6 g for the eastern Himalayas. Similarly, the expected minimum epicentral values of V_{peak} for $M_w = 8$ are 35 cm s^{-1} for the western and 112 cm s^{-1} for the eastern Himalayas. To understand whether our results reflect the properties of the subregions and not of a small data set, we check them against macroseismic intensity data for the same subregion. The presence of unusually high levels of epicentral amplitudes for the eastern subregion agrees well with the macroseismic evidence such as the epicentral intensity levels of X–XII for the Great Assam

* Now at: CSIR Centre for Mathematical Modelling and Computer Simulation (C-MMACS), NAL Belur Campus, Bangalore, 560037, India. E-mail: parvez@cmmacs.ernet.in

earthquake of 1897. Therefore, our results represent systematic regional effects, and they may be considered as a basis for future regionalized seismic hazard assessment in the Himalayan region. We see the location of earthquake sources/faults at a considerable depth within the relatively drier and higher-strength shield crust as the main cause of the observed enhanced amplitudes for the eastern Himalayas events. Western Himalayas sources are shallower and occupy the tectonically highly fractured upper part of the crust, of accretionary origin. The low attenuation common to both subregions is due to the presence of cold, low-scattering and high-Q shield crust.

Key words: attenuation, earthquake source, Himalayan region, seismic hazard, strong-motion amplitude.

1 INTRODUCTION

The Himalayan region in India is one of the most seismically active areas of the world. The region forms the collision plate boundary between the Indian and Eurasian plates and has experienced many great earthquakes ($M>8$) that have inflicted heavy casualties and economic damage. Hence, it is essential to assess the intensity of severe ground motion in order to specify appropriate structural design loads and to undertake other countermeasures. The determination of ground motion relationships describing peak ground acceleration and velocity as a function of magnitude and distance may represent an important step in solving this problem. During the last two decades, many researchers (e.g. Trifunac 1976; Joyner & Boore 1981; Kawashima *et al*. 1986; Sabetta & Pugliese 1987; Fukushima & Tanaka 1990; Ambraseys 1995; Atkinson & Boore 1995; Campbell 1997; Gusev *et al*. 1997) have studied the ground motion attenuation relationships for various regions of the world. Chandrasekaran (1994), Singh *et al*. (1996) and Sharma (1998) proposed attenuation relations for the Himalayan region. Most of these studies are, in essence, multiple regression models that permit the prediction of a target parameter by means of an empirical relationship established on the basis of the available strong-motion data from a particular region. However, even for regions with a long history of strong-motion observations, data are often not sufficient for obtaining completely reliable average trends.

Among the studies that characterize various regions of the territory of India, and in particular the Himalayan region, one should first mention the research on the attenuation of macroseismic intensity, based on isoseismal maps and available macroseismic data (e.g. Kaila & Sarkar 1977; Chandra 1980; Gupta & Trifunac 1988). Instrumental data for strong motion in the Himalayan region were not available before 1986, and this impeded the determination of attenuation relationships of peak ground motion based on local data. This is the reason why the attenuation relationships of other regions (e.g. eastern United States) were adopted for seismic hazard studies, in order to estimate the expected strong ground motion amplitudes (Khattri *et al.* 1984). In choosing a particular 'analogue region', it is required that both regions have similar attenuation with distance of the Modified Mercalli Intensity (MMI). Gupta & Trifunac (1988) used the probabilistic relations for the attenuation of MMI with distance in India and applied scaling equations for strong-motion parameters in terms of site intensity for some other regions, which have a similar definition of intensity. This approach is indirect, and the availability of even a limited instrumental data set justifies further analysis. Such an analysis will significantly improve the reliability of the evaluation of seismic hazard. As a first step in this direction, it is worthwhile determining region-specific attenuation relationships for peak amplitudes based on locally recorded strong-motion accelerograms.

In 1985–1986, three strong-motion arrays were installed in the Himalayan region. Six events with M_w in the range 5.2–7.2 were recorded by these arrays during 1986–1991. Recently, Sharma (1998) used these data to obtain the attenuation relationship for peak ground horizontal acceleration for the Himalayan region based on the multiple regression approach. However, in his work he excluded two major events from his study. This data censoring, with so small a data set, does not seem well justified. Formally, these data were excluded because of large source depths. We will show that these events do not differ from other events in any significant respect and essentially belong to the same population as the others. One additional reason why these data deserve repeated study is the unusually gradual distance decay of amplitudes found by both Singh *et al.* (1996) and Sharma (1998). Such a slow decay is not plausible from the physical viewpoint. Another less detailed study based on this data set is that of Chandrasekaran (1994). He also obtained a regional attenuation relationship but did not consider it as fully reliable. The main conclusion of his work was that a large amount of data is needed in order to develop a sufficiently accurate relationship.

In the present study, we analyse the strong-motion amplitudes obtained by the Himalayan arrays following the approach of Gusev (1983) and Gusev & Petukhin (1995, 1996). To determine the peak horizontal acceleration and velocity relationships with magnitude and distance, we prefer to combine the limited amount of available observations with theoretically based attenuation laws, rather than to seek for purely empirical relationships based on 'blind' multiple regression. Particularly dangerous in this situation is the so-called one-step regression approach (see Joyner & Boore 1981, 1993). The general approach that has been applied to the data includes the following steps: (1) reduction of the data to a fixed distance; (2) reduction of the result to a fixed magnitude; and (3) analysis of ground, subregional and station effects. In both reductions, a number of variants of the attenuation laws and magnitude trends have been investigated and the appropriate one, assumed to be near-optimal, was chosen. After accounting for the subregional effect, we derive the attenuation relationships for two subregions, the eastern and western Himalayas.

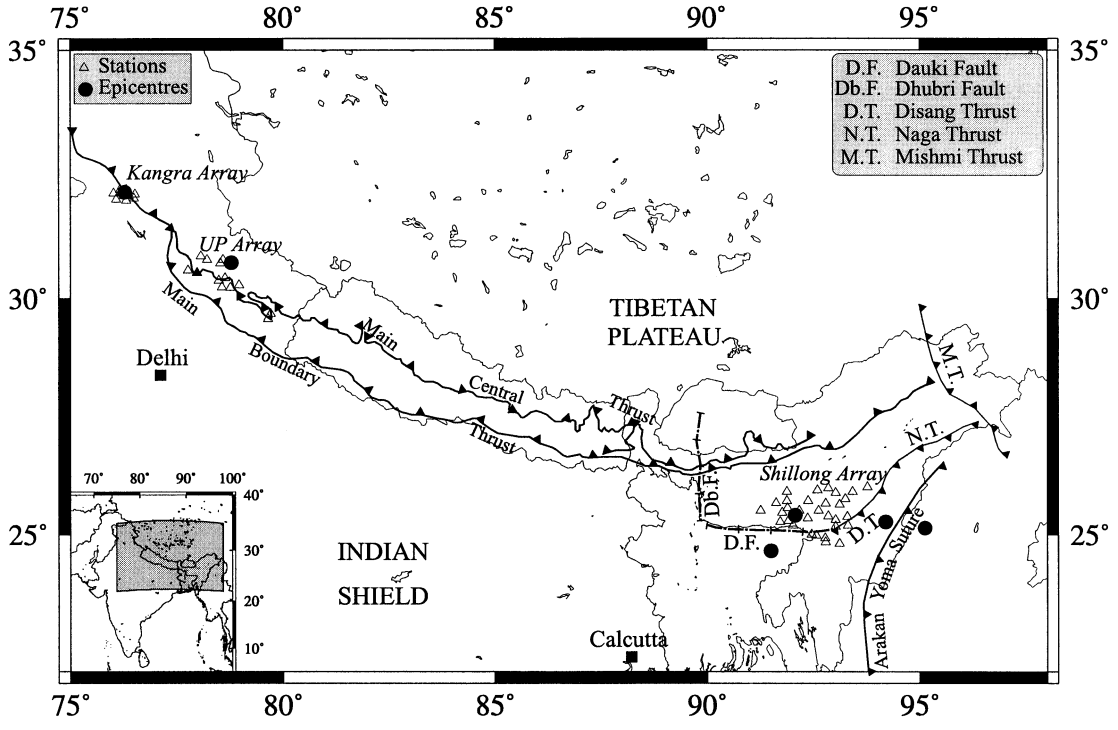

Figure 1. Generalized geological map showing the strong-motion arrays and the event locations in the Himalayas recorded by the network.

2 STRONG-MOTION ARRAYS AND DATA

The Department of Science and Technology (DST), Government of India, under the programme of Intensification of Research in High Priority Areas has funded three strong-motion arrays in India. The Department of Earthquake Engineering, University of Roorkee (Chandrasekaran & Das 1992), installed these arrays during 1985–1986. Fig. 1 gives the locations of these arrays, namely (1) the Shillong array (in the state of Assam and Meghalaya), (2) the Uttar Pradesh Hills (UP) array (in the west of the state of Uttar Pradesh), and (3) the Kangra array (in the state of Himachal Pradesh).

45 analogue strong-motion accelerographs have been installed in the Shillong array with a spacing of 10–40 km, 50 similar accelerographs were installed in the Kangra Array and 40 in the UP array with a spacing of 8–30 km. The instruments are three-component SMA-1, Kinemetrics, USA. Fig. 1 shows the locations of stations with instruments that have been triggered at least once. The epicentres of the recorded events are also shown. Four events with magnitude 5.2–7.2 were recorded by the Shillong array between 1986 and 1988 and two earthquakes with magnitude 5.5 and 6.8 were recorded separately by the Kangra and UP arrays in 1986 and 1991, respectively. Detailed information about the epicentral parameters of each event is listed in Table 1. As a measure of the source size we use the moment magnitude M_w. Five events have been taken from the Harvard CMT catalogue. For the event of 1986 September 10, M_w is not reported by any agency, but ISC gives $M_s = 4.5$, from which we estimate $M_w = 5.2$ (through the non-linear relationship compiled by Gusev 1991). We reject the possibility of using M_L as the reference magnitude because M_L determined for the region of study is not totally reliable.

The preliminary processing and digitization of the strong-motion records of these events was performed by Chandrasekaran & Das (1992). They used the baseline correction and filtering procedures of Lee & Trifunac (1979). The process is fundamentally the same as the standard processing method described by Hudson *et al.* (1971). The data were sampled at a rate of 0.02 s and they were bandpass filtered with characteristic frequencies of 0.17, 0.20, 25.0 and 27.0 Hz using an Ormsby filter. In the present study we use 138 horizontal-component

Table 1. List of events used in the study of A_{max} and V_{max}.

No.	Region	Date	Time (UT)	Lat. (°N)	Long. (°E)	Depth (km)		M_w
						(CMT)	(NEIC)	
1	W. Himalayas	1986 April 26	07:35:20.0	32.17	76.28	15	33	5.5
2		1991 Oct. 19	21:23:21.6	30.73	78.79	15	10	6.8
3	E. Himalayas	1986 Sept. 10	07:50:25.6	25.42	92.08	_	43	5.2
4		1987 May 18	01:53:59.3	25.27	94.20	75	50	6.2
5		1988 Feb. 6	14:50:43.6	24.64	91.51	31	33	5.8
6		1988 Aug. 6	00:36:37.6	25.14	95.12	101	91	7.2

peak accelerations and velocities (including both components) from the events recorded by the Shillong array and 44 horizontal-component peak accelerations and velocities from the Kangra and UP arrays. To represent relative site locations, we use the hypocentral distance. Detailed information of site conditions is not available. The sites of the Kangra and UP arrays are in the High Mountain terrain, which is expected to be devoid of thick alluvial cover, but the sites may be on gravel sediments in river valleys or on severely fractured and weathered rock. The site conditions of the Shillong array are even more complicated, with mixed rock and soil types. The altitudes of the sites of this array are much lower than the two former arrays.

A summary of data coverage with magnitude and hypocentral distance is shown in Fig. 2. Circles denote eastern Himalayan events and diamonds denote western Himalayan events. The same symbol convention is used throughout the text. The figure shows that our data coverage over hypocentral distance is very poor. Data for most events cover only a limited distance interval and for three events out of six, there are no data at distances below 90 km.

3 GEOLOGY AND TECTONICS

The general geological and tectonic location of the study area is shown in Fig. 1. For plate tectonic reviews of this area see e.g. Gansser (1964, 1977), Evans (1964), Valdiya (1980), Wadia (1975); a more traditional description of tectonics and seismogeology can be found in e.g. LeFort (1975), Mitchell (1981), Sinha-Roy (1982), Ni & Barazangi (1984), Chen & Molnar (1990). Based on these sources, we give here only a very brief resumé of the geology and tectonics of the region. The earthquakes under study occurred within two locations along a first-order tectonic feature. The two western events occurred in the collision boundary between the Indian and Eurasian plates. Here the Indian plate is assumed to subduct at a low angle under Tibet, and the main Himalayan range represents the prominent accretionary feature in this subduction system. The eastern group of four events is located in the northeastern region of India, which has undergone various stages of tectonic activity. The present-day tectonics of the region is complicated because of the interaction between active north–south convergence along the Himalayas and the east–west convergence and folding within the Indo–Burman ranges (Ni & Barazangi 1984). These four events are located about 200–250 km to the south of the main subduction boundary.

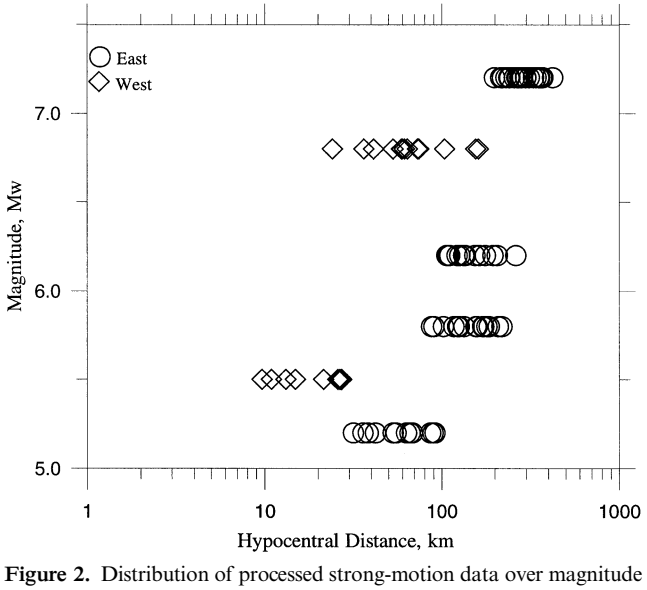

Figure 2. Distribution of processed strong-motion data over magnitude and hypocentral distance.

On a smaller scale, the two western arrays of Kangra and Uttar Pradesh Hills are located in the vicinity of two major faults, the Main Boundary Thrust (MBT) and the Main Central Thrust (MCT), that trace the entire length of the Himalayas. The MBT is a series of thrusts that separates the predominantly pre-Tertiary Lesser Himalayas from the Tertiary Siwalik belt (Wadia 1975; Gansser 1964, 1977). This zone comprises a mountain belt ranging in elevation from about 500–2500 m, composed of fossiliferous Riphean sediments overridden by several thrust sheets. The MCT at the base of the central crystalline zone (Gansser 1964) dips northwards, separating the High Himalayas from the Lesser Himalayas. Many stations of the UP array lie along the MCT. The MBT and MCT, which dip steeply (30°–45°) near to the surface, flatten out at depth and are assumed to merge to form the interplate surface dipping to the north at 15°. Many transverse faults and other secondary faults cutting across the Himalayas tectonic province have also been recognized. The famous Kangra earthquake of 1906 ($M=8.1$) occurred here and the Kangra array is located in its epicentral area.

The Shillong array is located on and around the Shillong Plateau. The Precambrian basement of the Indian shield is exposed on the Shillong Plateau and in the Mikir Hills to the northeast (Evans 1964), with an average elevation of 1000 m. These crystalline rocks are almost completely surrounded by Tertiary sedimentary rocks and Quaternary sediments of the Bengal basin to the south, of the Assam valley to the northeast and of the Brahmaputra valley to the north (Evans 1964; Mitchell 1981). The eastern boundary of the Shillong Plateau and the Mikir Hills abuts against the northern part of the Indo–Burman ranges, which locally trends northeastwards and joins the eastern Himalayas to form the Assam syntaxis. The Shillong Plateau is bounded by prominent tectonic features, for example, the Dhubri fault towards the west and the Dauki fault towards south. The Dauki fault merges with the northeast-trending Disang and Naga thrusts towards the east (Fig. 1). This region has experienced some of the world's biggest earthquakes. The 'Great Assam' earthquakes occurred in the Shillong region in 1897 ($M=8.7$) and in the Mishmi region in 1950 ($M=8.6$). The Shillong array approximately covers the epicentral area of the 1897 event.

4 SIMPLE THEORY VERSUS EMPIRICAL FORMULAE IN STRONG-MOTION DATA ANALYSIS: MODELLING MAGNITUDE-DEPENDENT ATTENUATION FOR SEMI-EMPIRICAL DATA ANALYSIS

Let us consider in what form we should seek the description of the observed accelerations and velocities. In a region with a sufficiently large amount of recorded strong-motion data, the average dependence of strong-motion parameters (e.g. peak acceleration) on distance, magnitude and other parameters is usually determined on an empirical basis by means of multiple regression procedures. Theoretical considerations are only used,

if at all, in choosing the form of the regression formula. Such empirical formulae (not always mutually compatible) are then used for approximate forecasting of various parameters of strong ground motion related to specific earthquake sources, wave propagation paths and site geology. One difficulty with such formulae is related to the discrepancies between simple forms of traditional empirical regression relationships for various ground motion parameters and the actual, often non-linear, trends that are both observed and expected from even a simple theory. For example, until 1985 the regression coefficient that defined amplitude attenuation was almost never (even implicitly) assumed to be magnitude-dependent, whereas such a dependence is evident in the data, and it arises automatically in an adequate theoretical calculation. The situation is frequently aggravated by a very limited number of observations in many poorly studied and/or low-seismicity areas. To formally describe non-linearities or interactions between factors one needs a considerable number of regression coefficients, but the data may barely be sufficient to determine two or three. To replace the use of formulae, we designed a simplified practical algorithm capable of determining approximate mean trends of strong ground motion parameters. To make these trends more reliable, we specify many properties of Earth medium and earthquake sources (where possible) in a way that is independent of scarce strong-motion data. The trends calculated in this manner may be used instead of formulae, both in the analysis of observed ground motions and in the construction of predictive schemes that interpolate or extrapolate the data. This approach is particularly valuable when used for extrapolation because it gives at least a limited guarantee against grossly erroneous predictions. Of course, it can produce errors but they are much more 'controllable', because the simplifications made in the modelling are explicit, in contrast with the implicit assumptions made when choosing a particular structure of an analytic formula. To implement the approach described, a dedicated code (SSK) has been developed (Gusev & Petukhin 1995, 1996) and a brief description of it is given in the Appendix. In a number of aspects, our method of data analysis follows the approaches of Trifunac (1976) and Trifunac & Lee (1990).

The mode of data analysis described seems especially appropriate for the present study when the data coverage over distance and magnitude is poor and purely empirical analysis is hardly possible at all. Therefore, we will use a simple theoretical model to describe the attenuation of peak acceleration and velocity in a magnitude-dependent way. At a given magnitude, we can determine the shape of the distance, R, dependence on a theoretical basis and then adjust only its absolute level to the data. In practice, an equivalent procedure has been applied: data have been reduced to a fixed distance and magnitude and then averaged.

5 DETERMINATION OF THE EMPIRICAL REGIONAL $A_{max}(M_w, R)$ RELATIONSHIP

5.1 Choosing the model scaling law of the source spectra for predicting peak acceleration trends

As an initial step in the data analysis, we compare the theoretical curves of the distance decay of the peak acceleration (cm s^{-2}) and velocity (cm s^{-1}), calculated with the SSK code, to a set of empirical relationships. We confine this comparison to two magnitude values, $M_w = 5.5$ and 7.5. To specify the source effect, two $K(f)$ scaling laws have been used: those after Gusev (1983) and Brune (1970) with the modifications of Joyner (1984). In Fig. 3, the solid curves correspond to $M_w = 7.5$ and the dashed curves to $M_w = 5.5$. The theoretical curves correspond to the following set of model parameters: $R_c = 70$ km, $n_a = 1$, $n_b = 0.5$, $Q_a = 300$, $Q_b = 300$ and $\gamma = 0.62$, referred to below as ATT1. Here R_c is the critical distance where the attenuation curve changes from an approximate body wave style ($1/R$) to a surface wave style ($1/\sqrt{R}$), Q_a is the quality factor for the first ($R < R_c$) branch of the attenuation curve, Q_b is the same for the second branch ($R > R_c$) and γ is the value of the exponent in the assumed power law of $Q(f)$ (see the Appendix for details). This set of values is based on the estimates derived from the abundant data set available for continental Northern Eurasia (Gusev & Shumilina 2000). The empirical mean peak acceleration and velocity curves are from Joyner & Boore (1981) for California, from Fukushima & Tanaka (1990) and Kawashima *et al.* (1986) for Japan and from Campbell (1997) for the worldwide data set. One can see from these figures that both Gusev's and Brune's spectral models, combined with the ATT1 model, predict the shape of distance decay quite realistically. The absolute values predicted by Brune's model are too low because we set the standard stress drop value to 50 bar. Gusev's spectral model is conservative for $M_w = 7.5$ and has been chosen for use in the following data analysis.

5.2 Reduction of the observed A_{max} values to the distance $R = 100$ km

In order to determine the absolute level of the $A_{max}(M_w, R)$ relationship, we reduce the observed peak acceleration values to a common hypocentral distance of $R = 100$ km by means of the following theoretical relationship:

$$A_{DR} = \left(\frac{A_{theo}(M_w, R = 100)}{A_{theo}(M_w, R)} \right) A_{max}^{(observed)}, \quad (1)$$

where A_{DR} is the reduced peak acceleration at the hypocentral distance $R = 100$ km, $A_{theo}(M_w, R = 100)$ is the theoretically calculated value of the peak acceleration at 100 km, $A_{theo}(M_w, R)$ is the theoretically calculated value of the peak acceleration with hypocentral distance R and $A_{max}^{(observed)}$ is the observed peak acceleration. The quality of the fit in the distance reduction has been determined as the average σ_{DR}^2 of the six estimates of the sample variance $\sigma^2(A_{DR})$, determined individually for each event. This was done initially using the theoretical distance attenuation model ATT1, which produced $\sigma_{DR}^2 = 0.050$. The analysis of the residuals has shown that this model is not completely adequate since the distance decay is somewhat too steep when compared to observations. This is quite understandable because this empirical model is based on data recorded in other regions. To rectify this deficiency we assume the presence of very high Q (combined with the crustal high-frequency waveguide effects already assumed). We thus change the parameters of the second branch of our attenuation law and use the highest possible value of $Q_b = 1200$ combined with $\gamma = 0.40$ (this variant is denoted by the ATT2 model). The residual scatter is reduced to $\sigma_{DR}^2 = 0.048$ and the behaviour of the residuals does not show any systematic feature; therefore, we consider the fit obtained to be acceptable.

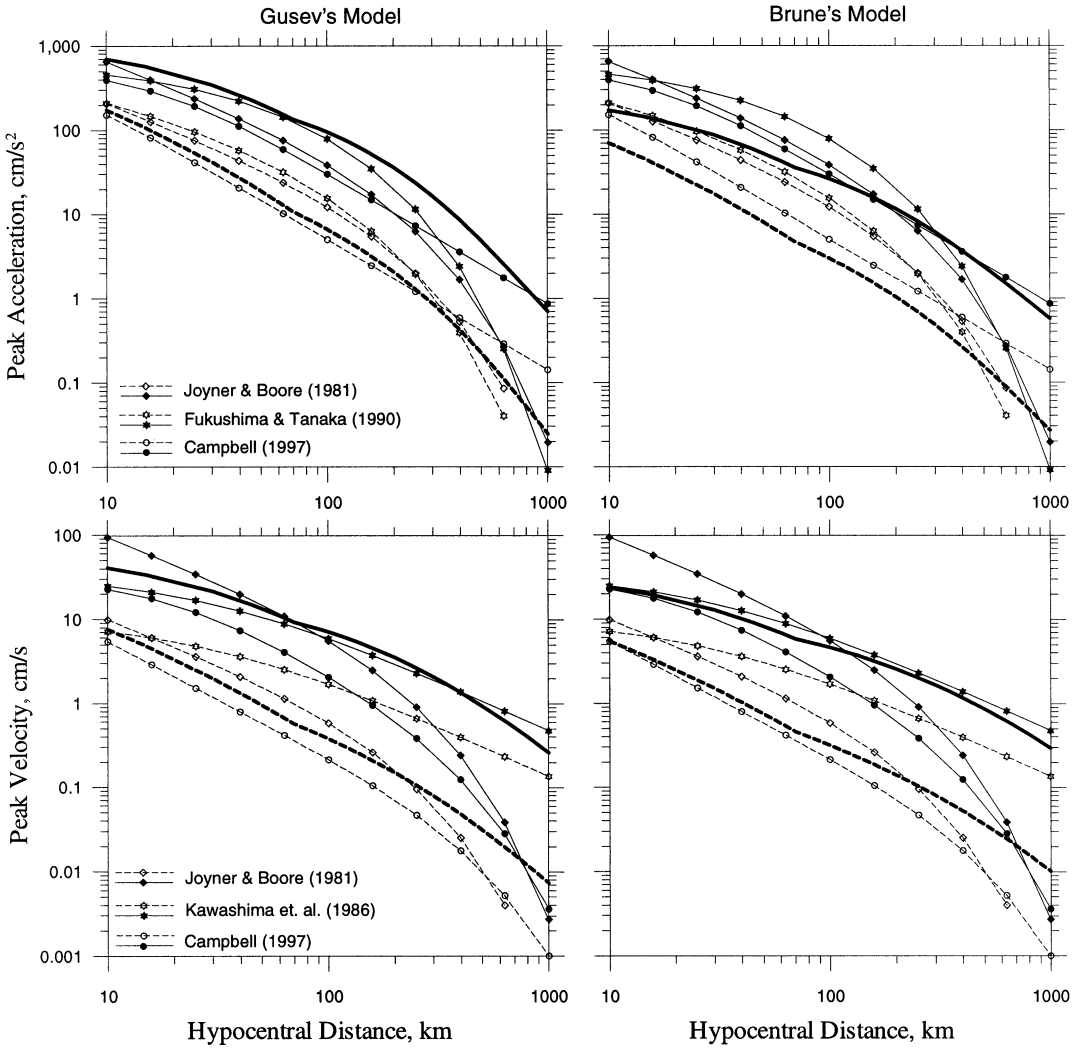

Figure 3. Theoretical curves of the distance decay of the peak acceleration and velocity based on the Gusev (1983) and Brune (1970) models. The thick solid and dashed lines correspond to $M_w = 7.5$ and 5.5, respectively. The empirical mean peak acceleration and velocity curves from other authors are represented by thin lines with solid and open symbols for magnitudes of 7.5 and 5.5, respectively.

The reduced amplitudes are shown in Fig. 4(a). In Fig. 5, we show the residuals of this fit for peak acceleration and velocity. For most of the events, the fit is visually quite acceptable.

Nevertheless, to ensure against the possibility of the complete inadequacy of our theoretical model, we perform a more traditional and empirical regression of our data. It emulates the first step of the two-step regression (Joyner & Boore 1981, 1993). We assume a simple hyperbolic law (r^{-n}) for the amplitude decay and we estimate the value of the exponent n. Like Sharma (1998), we use least-squares regression with dummy variables to decouple the interfering effect of the event size, and obtain $n = 1.25$, which is very near to Sharma's figure. In this case, the residual error is $\sigma^2_{DR} = 0.047$. Our final choice for the distance reduction is based on the theoretical attenuation model ATT2.

5.3 Choice of the $A_{max}(M_w)$ relationship and determination of the absolute level of A_{max} (M_w, R) at $R = 100$ km, $M_w = 7$

In Fig. 4(a), we showed the reduced data $A_{DR} = A_{max}(M_w, 100)$ versus the moment magnitude M_w. To perform the next step of our analysis we have to determine the particular A_{DR} versus magnitude relationship to be used in the reduction over magnitude. This is an important issue, and we consider three possibilities: performing an empirical regression; using a theoretically calculated curve; and adopting an empirical curve determined for another region. We will start with the empirical linear regression. We immediately note that the largest event ($M_w = 7.2$) seems to be an outlier (Sharma 1998). We thus perform the regression using either all six events of the total Himalayan territory (TH-6) or only five events (TH-5), excluding the $M_w = 7.2$ event (see Fig. 4a). The residual rms deviation of decimal log data is found to be 0.37 for TH-6 and 0.36 for TH-5; the difference is small and gives no support for the exclusion of the $M_w = 7.2$ event. The most remarkable feature is the absolute value of the residual error, which is much larger than typically observed values, which are usually within the range 0.15–0.30 in terms of $\log_{10} A_{max}$.

In an attempt to explain the large scatter in our data, we first try to analyse possible station/site effects, but the network does not provide the site condition of each station. We therefore try to use the site information provided by Sharma (1998), and repeat the distance attenuation analysis with a least-squares

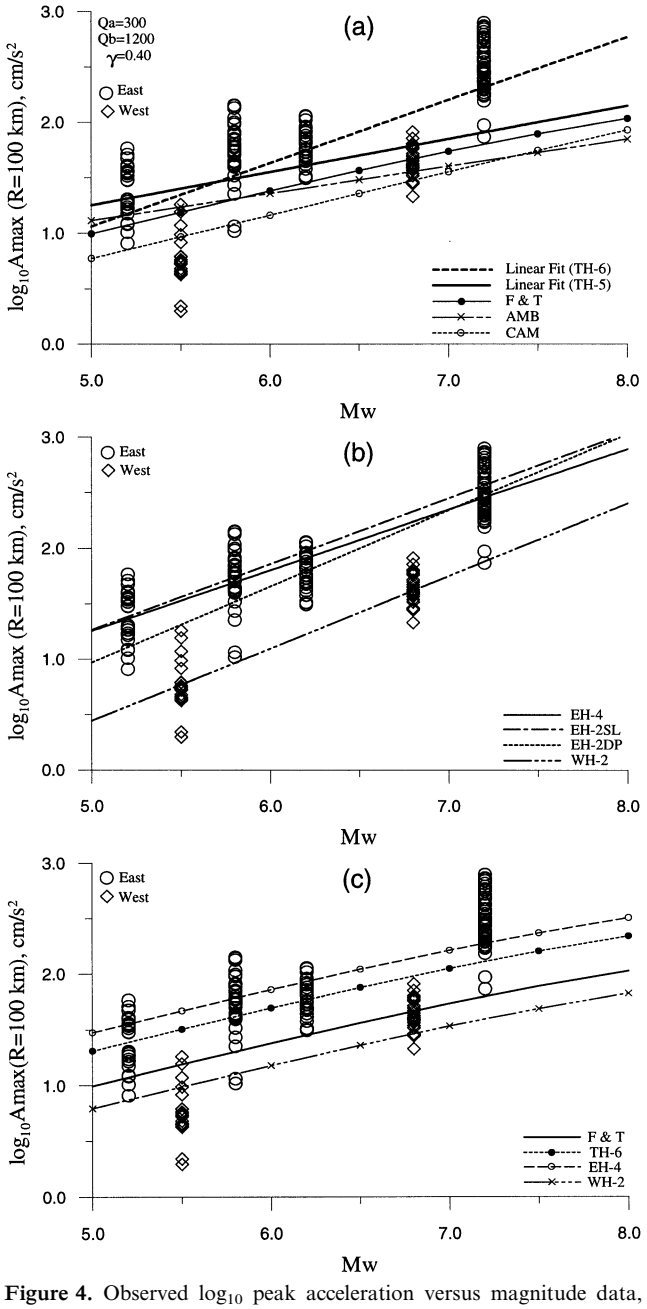

Figure 4. Observed $\log_{10}$ peak acceleration versus magnitude data, after reduction to 100 km, using the ATT2 model (see text). Circles correspond to the events of the eastern Himalayas and diamonds to the events of the western Himalayas. TH-6: all six Himalayan events; TH-5: five Himalayan events excluding the largest event with $M_w = 7.2$; EH-4: four eastern Himalayan events; EH-2SL: two shallow eastern Himalayan events (see Table 1 for depth values); EH-2DP: two 'deep' eastern Himalayan events; WH-2: two western Himalayan events; F & T: Fukushima & Tanaka (1990); CAM: Campbell (1997); AMB: Ambraseys (1995).

regression with the additional dummy variable describing the ground type. However, this approach does not yield satisfactory results because (1) some of the stations are specified ambiguously, and (2) ground-type terms obtained in the tentative regression are negligible not only for A_{max} but also for V_{max}, casting even more doubt on the results of such an analysis.

However, there is another possible explanation, namely that the data are generally non-homogeneous. To test this idea, we divide the data into groups and process them separately. First we group data on the basis of region. The results are shown in Fig. 4(b), where we give the regression lines for the two regional groupings: four eastern events (EH-4) and two western events (WH-2). The residual rms deviations for EH-4 and WH-2 are 0.23 and 0.19, respectively. This is a radical reduction of the scatter of data (compared to 0.37 for TH-6), and a separate analysis of data region by region seems necessary. We also divide the EH group into two on the basis of focal depth: two shallow events (EH-2SL) and two deeper ones (EH-2DP) (see Table 1 for the depth values and Fig. 4b for the linear fit). For the two groups EH-2SL and EH-2DP, the rms deviations are 0.25 and 0.21, respectively (note that the $M_w = 7.2$ event is included in the EH-2DP group). Separating the data over depth does not result in a marked effect on the fit, and the assumption that the $M_w = 7.2$ event is an anomaly remains totally groundless. Therefore, will conduct the analysis below considering two groups of data, the eastern and western Himalayas.

In Fig. 4(a) we have plotted the M_w dependence of mean empirical $\log_{10} A_{max}$ at $R = 100$ km from Fukushima & Tanaka (1990), Campbell (1997) and Ambraseys (1995) for Japan, worldwide earthquakes and Europe, respectively. One can see from the figure that the slope of our linear fit for TH-6 does not match the results obtained for the other regions; it also contradicts theoretical estimates based on realistic spectral scaling laws. However, the data volume (essentially six points) is prohibitively low even for the TH6 group, where the inhomogeneous character of the data makes the meaning of the result doubtful anyway. For smaller groups, the regression is evidently meaningless. Hence, we conclude that our data are completely inadequate for the determination of the magnitude dependence. For this reason, we choose to use the empirical magnitude trend (not the absolute level) from another region. In particular, we employ the empirical shape of Fukushima & Tanaka (1990) (F & T) as the one that is the best supported by large-magnitude data. We also considered the use of a theoretically calculated magnitude trend, but we rejected this option in favour of the empirical one, considering such an approach more conservative. There are examples when reasonable theoretical spectral scaling laws make incorrect predictions of A_{max} versus magnitude trends (see e.g. Singh *et al.* 1989).

Having chosen the shape of the magnitude trend, we can now perform the second step of the analysis and reduce A_{DR} data along the magnitude axis to a fixed magnitude value, $M_w = 7$. The magnitude reduction can be expressed by the following formula:

$$A_{MR} = \left(\frac{A_{\text{trend},R=100}(M_w = 7)}{A_{\text{trend},R=100}(M_w)} \right) A_{DR}(M_w) . \quad (2)$$

The notation is similar to eq. (1), except that this time we reduce A_{DR} to a fixed magnitude $M_w = 7$. This step is shown in Fig. 4(c). In this figure, we show the F & T curves adjusted vertically to the average reduced amplitudes A_{DR} for TH-6, EH-4 and WH-2, and the original F & T curve. The values of the residual error, which now coincides with the rms deviation of A_{MR}, are slightly increased compared to the case of the linear fit, and are equal to 0.40, 0.27 and 0.26, respectively.

The absolute levels of peak acceleration obtained are of interest. The difference between the group averages is unexpectedly large. For the western Himalayas events, the level

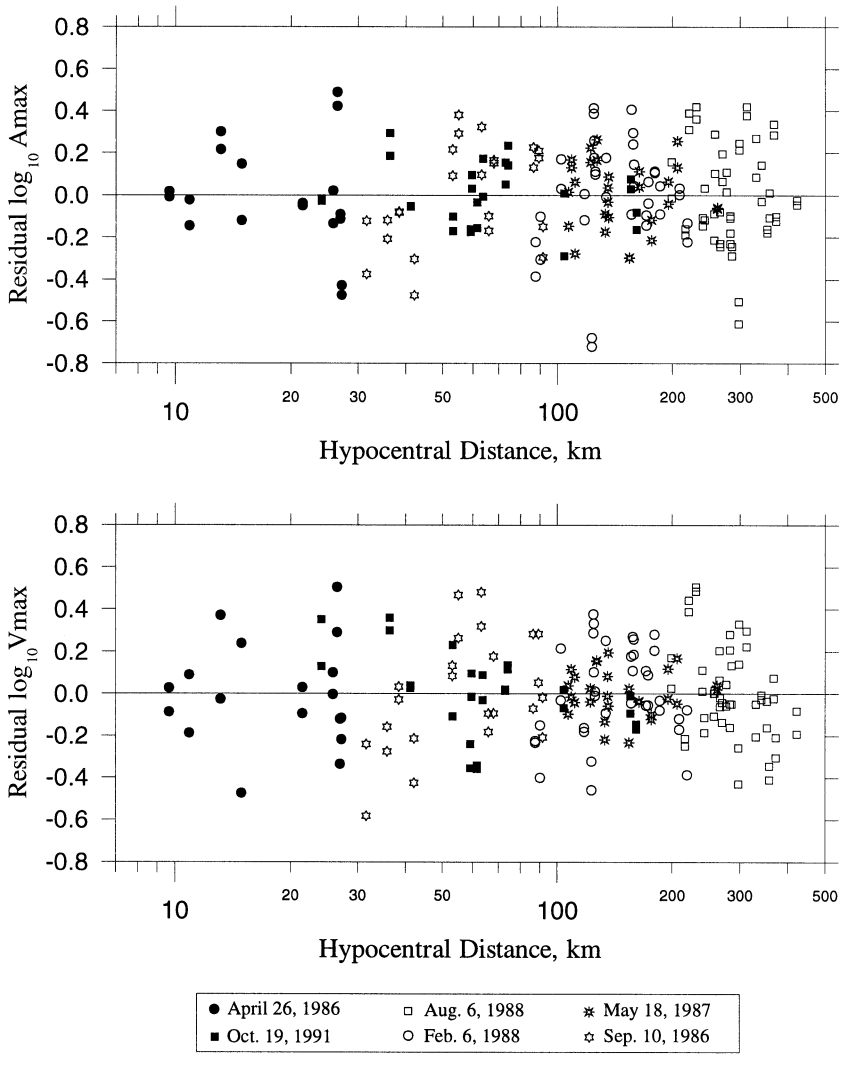

Figure 5. The residuals of the $\log_{10}$ peak acceleration and velocity data reduced using the model ATT2 as a function of the hypocentral distance. Different symbols are used for different events.

is about 62 per cent of the F & T level, whereas for the eastern Himalayas events it is about three times this reference value. The results obtained at this stage are essentially final: we have determined our expected $A_{\max}(M_w, R)$ relationship for the western and eastern Himalayas. It is defined by (1) the absolute reference values $A_{MR} = A_{\max}(7,100) = 35$ and 150 Gal, respectively, and (2) our procedure, which, applied in reverse order, determines first the $A_{\max}(M_w, 100)$ and then the $A_{\max}(M_w, R)$ relationships tied to these 'anchors'.

5.4 $A_{\max}(M_w, R)$ relationship as an extrapolation of observations to small distances and large magnitudes

We have established the semi-empirical relationship $A_{\max}(M_w, R)$, and formally we could consider the analysis completed, but it is of interest to observe what our results mean for small distances and large magnitudes. In Fig. 6(a) we represent our results as two families of $A_{\max}(R)$ curves for a set of M_w values. Thin solid curves are our predicted values for the eastern Himalayas and thin dashed curves are for the western Himalayas. Each event of our very modest database is represented by its centroid (dot) and by a segment describing the data range. All segments have the common slope of -1.25 found in the previous section. Our curves represent quite a reasonable description of observational data for peak acceleration from both regions.

To make an additional check, we show in Fig. 6(b) the result of an empirical analysis based on the assumption of the hyperbolic law ($R^{-1.25}$) for the distance decay, with the same reference values at $R = 100$ km as those in Fig. 6(a). We stopped our straight lines for $M_w = 7$ and 8 at the level of $A_{\max} = 1800$ Gal because the epicentral zone corresponds roughly to the distance range 20–60 km for the (deeper) EH events, and to the distance range 10–30 km for the (shallower) WH events, and we do not consider this kind of extrapolation to be reliable. We see that even after accounting for amplitude saturation near to the source, the eastern Himalayas earthquakes of $M_w = 7$–8 must be expected to regularly produce horizontal peak accelerations of 1–1.5 g in the vicinity of the seismogenic fault.

In Fig. 7 we compare our results for expected $A_{\max}$ versus hypocentral distance to the results obtained by other researchers for fixed $M_w = 7$ (or $M_L = 6.7$). The thick solid line represents our results for the eastern Himalayas and the thick dashed line our results for the western Himalayas. Solid symbols mark the curves for the Himalayan region obtained by Chandrasekaran

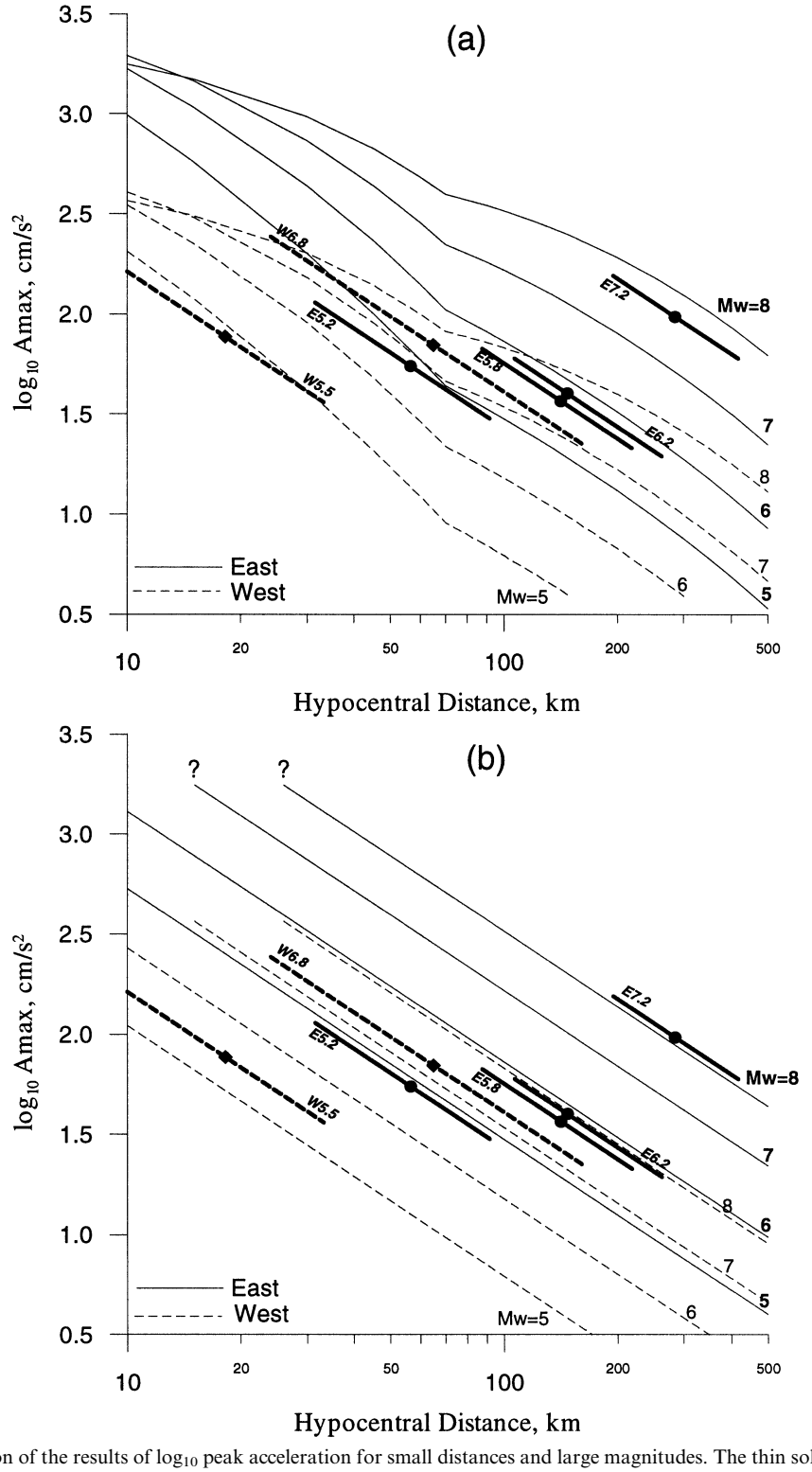

Figure 6. (a) Extrapolation of the results of $\log_{10}$ peak acceleration for small distances and large magnitudes. The thin solid curves are the predicted values for the eastern Himalayas and the thin dashed curves are for the western Himalayas. The thick solid and dashed lines are the segments of the observed data with their centroids for the eastern and western Himalayas, respectively. (b) Results of the empirical analysis based on the assumption of the hyperbolic law ($R^{-1.25}$) for distance decay, with the same reference values at $R = 100$ km as those in (a).

(1994), Singh *et al.* (1996) and Sharma (1998) on the basis of essentially the same strong-motion data set as the one used in the present study. Open symbols denote the results from other parts of the world, namely Trifunac (1976) and Joyner & Boore (1981) for the western USA, Ambraseys (1995) for Europe, Atkinson & Boore (1995) for eastern North America and Fukushima & Tanaka (1990) for Japan. One can see from this figure that our result for the eastern Himalayas is unusually high compared to all the others except for that of Chandrasekaran (1994), whereas our results for the western Himalayas are

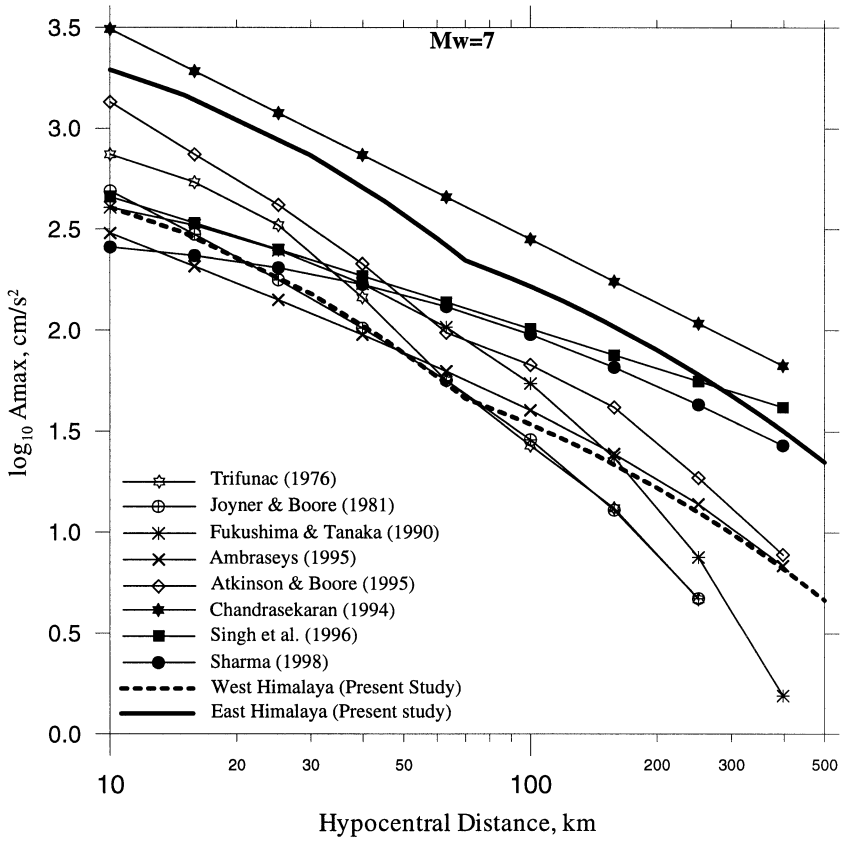

Figure 7. Comparison of our results for expected $\log_{10}$ peak acceleration versus hypocentral distance with those of other authors. Our results are shown as a thick solid line for the eastern Himalayas and a thick dashed line for the western Himalayas for $M_w = 7$. The thin curves with solid symbols are from the Himalayan region, while the thin curves with open symbols are from different authors for different regions of the world.

comparable to the others. Singh *et al.* (1996) and Sharma (1998) used the data from both subregions jointly; their results for $M_w = 7$ are close to our eastern Himalayas results for distances above 150 km and to our western Himalayas results for distances below 50 km. We believe that the main cause of the differences between these results and ours is our decision to split the data set into two groups, and we consider our results more reliable. Our results for the western Himalayas are comparable to those of Ambraseys (1995) for Europe and Joyner & Boore (1981) for California at $R < 100$ km. However, at $R > 100$ km the distance attenuation curve for California decays much faster than ours. At smaller distances, Fukushima & Tanaka's (1990) results are slightly above ours for the western Himalayas and lower than ours for the eastern Himalayas. The distance decay of the Fukushima & Tanaka (1990) trend at $R > 100$ km is much faster than ours. The closest analogue of our eastern Himalayas result, in terms of both level and shape of attenuation curve, is the trend of Atkinson & Boore (1995) for the eastern USA.

5.5 Statistical testing of the validity of the regionalization

Although the improvement of the fit after splitting the data into subregions is evident, some doubts may well remain because of the very limited amount of events. We therefore checked the validity of this splitting by analysing the variance of the residuals. Table 2 contains all relevant input information for $A_{max}(7,100)$ (and also for velocity, used later). Formally, we first wish to demonstrate that the value of the variance for all the data analysed together ($\sigma^2_{TOT} = 0.160$ when considering 182 observations, with 181 degrees of freedom, df) is significantly above the value of the variance for the data divided into the groups EH and WH ($\sigma^2_2 = 0.073$ when taking the average of the variance of the EH and WH groups considering the same 182 observations with 180 df). All quoted values are again in $\log_{10}$ units. Fisher's F-ratio (the ratio of the variance of two variables) is equal to 2.18 and it is above unity at a significance level above 10^{-5}. Thus, the gain in the fit is real, and the mean values of the two groups do differ.

However, one may question the meaning of this fact because it is possible that the particular distribution of six events into two regions is such that the occurrence of both low-amplitude events in the WH region is due to chance. Indeed, the probability of the two lowest-amplitude events occupying a particular two-event subgroup among six events is quite considerable ($2 \cdot 4!/6! = 1/15$). We try to answer this kind of criticism by analysing not individual station values but event averages. We must now compare the following two variance estimates: (1) one calculated for the average of the group of six events taken together (0.152), and (2) the average value of the two variance estimates calculated for the EH and WH subgroups (0.048). The improvement of the fit produced by such data splitting is drastic, with the variance reduction expressed by an F-ratio of 3.16. Unfortunately, with as few as 5 and 4 df this seemingly high value provides a significance level that does not even reach 10 per cent ($F_{5,4,90\,\text{per cent}} = 4.05$). Thus, the common-sense position is quite justified here: despite a real,

Table 2. Initial data used for the determination of the structure of variance for A_{MR} and V_{MR}*.

	Individual events							Regional groups			Joint data
	1	2	3	4	5	6	E§	WH 2	EH 4	R¶	
N	18	26	50	28	36	24		44	154		198
Acceleration data, log A_{max}(7, 100)											
m†	1.317	1.687	2.415	2.075	2.171	2.049	1.952	1.535	2.218	1.876	2.054
s^2‡	0.063	0.021	0.056	0.027	0.065	0.056	0.048	0.070	0.075	0.073	0.160
s	0.250	0.143	0.237	0.164	0.255	0.236	0.214	0.265	0.274	0.270	0.399
Velocity data, log V_{max}(7, 100)											
m†	0.369	0.549	1.061	0.889	1.021	0.861	0.841	0.476	0.981	0.728	0.859
s^2‡	0.060	0.039	0.048	0.012	0.048	0.072	0.047	0.054	0.051	0.053	0.099
s	0.245	0.197	0.219	0.109	0.220	0.269	0.210	0.233	0.226	0.230	0.314

* All columns except those denoted 'mean' contain averages over all stations that recorded the event or the group of events. Only data for near-optimal medium model ATT2 ($Q_a = 300$, $Q_b = 1200$) are listed. N is the number of records in each data group.
† Sample average log A_{max}(7, 100) or log V_{max}(7, 100).
‡ Sample variance.
§ Mean over six columns for individual events.
¶ Mean over two columns for individual subregions.

large difference between *regional data groups*, we do not have a fully convincing proof that this fact indicates a difference between *regions as such*. An additional, independent check is crucial; it is performed below based on macroseismic data.

Having split the data into subregional groups, we obtain an acceptable value of the residual variance $\sigma^2 = 0.073$ (or $\sigma = 0.27$). We can try to split this variance value further into two components: (1) the event-related component, rooted in variations of the radiation capability of the events, and (2) the residual component, which includes individual site conditions between stations, and also some uncontrollable random ingredients that include the effects of ray paths, purely stochastic effects and so on. We believe that the residual component is related, to a large extent, to individual station site effects, and we will refer to it as the station-related effect. It is of interest to isolate these two components of the total variance. The isolated station-related component is given in the E column of Table 2; it is equal to 0.048 (or $\sigma = 0.22$). We can now find the event-related component merely by subtraction, to obtain 0.073–0.048 = 0.025 (or $\sigma = 0.16$). For completeness, we quote the subregion-related component as well: $\sigma^2 = 0.160$–$0.073 = 0.087$ (or $\sigma \approx 0.29$).

6 DETERMINATION OF THE EMPIRICAL REGIONAL $V_{max}(M_w, R)$ RELATIONSHIP

The approach described above developed for the analysis of $A_{max}(M_w, R)$ has been applied to the peak velocity data in a very similar way, so we will report the results very briefly. The data again suggest the use of the ATT2 theoretical curves for the distance reduction, producing a residual error of 0.22 in the fit with the event effect excluded. The residual of this fit can be seen in Fig. 5. For the sake of comparison, a purely empirical way for the determination of the attenuation has been followed, and through a linear regression with dummy event variables we obtain again the exponent value $n = -1.18$ for the hyperbolic attenuation law, and a residual rms of 0.21.

We reduce the observed peak velocity (cm s^{-1}) data to $R = 100$ km using eq. (1) and the ATT2 model, and to determine the magnitude dependence (Fig. 8a) we first use the groupings TH6 and TH5 (excluding the event with $M_w = 7.2$, which again appears to be an outlier). The residual rms scatter is practically identical (0.31) for both TH-6 and TH-5. To reduce this scatter, we split the data into groups on the basis of the geographical region and focal depth. Fig. 8(b) shows the linear fit of $\log_{10} V_{max}(R = 100$ km) for EH-4, WH-2, EH-2SL and EH-2DP. The resulting residual rms deviations are 0.21, 0.25, 0.24 and 0.19, respectively; therefore, there is a large improvement in the results from the regional grouping and no improvement in the results from the depth grouping. Consequently, we decided to analyse separately the peak velocity data for the two regions of the eastern and western Himalayas.

The empirical $\log_{10} V_{max}(R = 100$ km) values from Kawashima *et al.* (1986), Joyner & Boore (1981), Atkinson & Boore (1995) and Campbell (1997) are shown in Fig. 8(a) for comparison. We consider our empirical trends unreliable, and we chose to use the empirical shape of the M_w versus V_{max} relationship of Joyner & Boore (1981). The resulting trends ['anchored' to the reduced V_{max}(7,100) value] accompanied by the original curves of Joyner & Boore (1981) are shown in Fig. 8(c) for TH-6, EH-4 and WH-2. The result for WH-2 is very close to that of Joyner & Boore (1981), while for EH-4 the intercept is about three times larger.

The established semi-empirical relationships $V_{max}(M_w, R)$ for EH and WH are represented in Fig. 9 as two families of $V_{max}(R)$ curves for $M_w = 5$, 6, 7 and 8. The solid thin lines are our expected trends for EH, and the dashed lines are those for WH. The data centroids (dots) and the distance ranges (thick segments) with an empirically determined slope of -1.18 are shown in the figure. The differences in the absolute levels of the expected peak velocity between regional groups are prominent, although not as large as that for peak accelerations (Fig. 6). The agreement between the predicted lines and the observed peak velocity from each event is quite acceptable. We can now compare our expected V_{max} versus hypocentral distance relationship with published trends for other regions (see Fig. 10, which is the same as Fig. 7 for A_{max}). We believe that the ground is rock for WH stations and mixed rock and hard soil for EH stations, in agreement with Sharma (1998). For comparison, we give the curves of Trifunac (1976, average for rock and medium

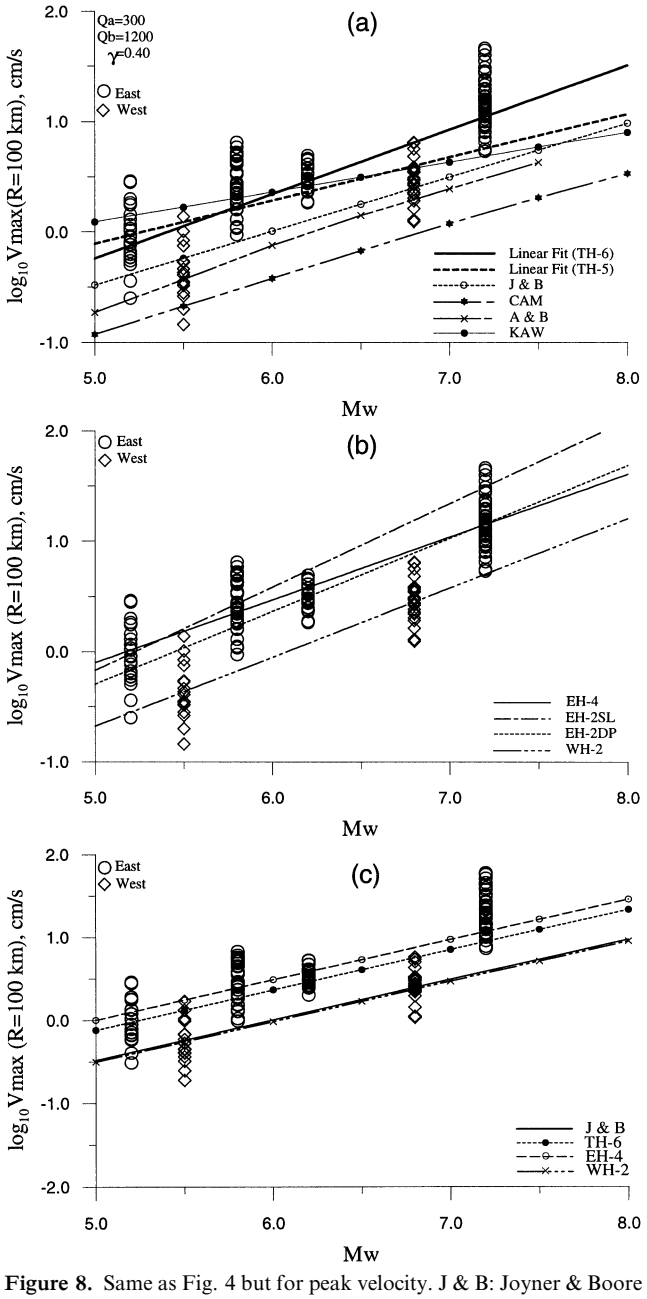

Figure 8. Same as Fig. 4 but for peak velocity. J & B: Joyner & Boore (1981).

ground) and Joyner & Boore (1981, hard soil) for the western USA, Atkinson & Boore (1995, typically rock type) for eastern North America, Kawashima *et al.* (1986, average for hard and medium ground) for Japan, and the world average of Campbell (1997, presumably rock). We see again that our result for the eastern Himalayas is unusually high, above all the others at distances in excess of 50 km, whereas our results for the western Himalayas look quite regular.

We have also performed a statistical analysis of residuals. The gain in the residual variance attained by splitting the data into subregional groups is measured by a somewhat smaller *F*-ratio value of 1.87, which is still significant at the 10^{-5} level (for 180 df). All this variance seems to be produced by station/site effects; the event-related contribution to the variance for velocity data is not observable. The value of the residual rms deviation is slightly smaller than for acceleration (about 0.23, compared to 0.27). The geological conditions of the stations have limited variations.

7 MACROSEISMIC EVIDENCE OF UNUSUALLY HIGH STRONG-MOTION AMPLITUDES IN THE EASTERN HIMALAYAS

Macroseismic data represent an independent data source that may help us to understand whether the large accelerations and velocities predicted by our analysis for the eastern Himalayas are the result of the peculiarity of our very small data set, or whether they are a real, systematic property of large earthquakes in this area. To perform such an analysis we need a measuring tool that might substitute for magnitude. It is common knowledge that the so-called epicentral intensity I_0 does not provide an efficient tool of this kind. Much more useful is the parameter I_{100}, or mean intensity at a distance of 100 km. This direct analogue of magnitude was introduced and effectively used by Kawasumi (1951) and later by Rautian *et al.* (1989). Recently, Gusev & Shumilina (2000) determined I_{100} for more than 300 large earthquakes of the territory of Continental Northern Eurasia (CNEA, i.e. former USSR with Kurile–Kamchatka excluded). They determined a very stable I_{100} versus M_w ($I_{100}-M_w$) relationship that can easily be used as a reference for the analysis of the macroseismic data for a particular region.

To understand how the Indian data behave with respect to this reference data set, we determine I_{100} values for a number of earthquakes located in various parts of India and, for comparison, in some other regions of the world, using the published results of Chandra (1979, 1980), Chandra *et al.* (1979), Tilford *et al.* (1985) and Erdik *et al.* (1985). These authors represented their results using the value of I_0 (see Table 3), but this is not an observable entity; instead it is a parameter that describes the observation determined by some graphical data fitting and thus is not necessarily an integer (Chandra *et al.* 1979). In Fig. 11, the three parallel curves represent the mean $I_{100}-M_w$ trend (thick lines) $\pm 1\sigma$ (thin lines) for CNEA. The thick dashed line is the trend determined for Japanese events compiled by Gusev & Shumilina (2000), which matches the trend of the CNEA data unexpectedly well. The thin line with open symbols shows the trend of California after Lee & Trifunac (1985), but this is valid only for magnitude less than 7. We have also plotted the $I_{100}-M_w$ line for 'stable continental regions' derived from Table 3 of Johnston (1996b). Large symbols denote I_{100} values evaluated for several events through a combination of the published I_0 values and the published empirical distance attenuation formulae (for I_0) valid for different regions such as the eastern Himalayas, the western Himalayas, Bihar Nepal, Peninsular India, Central USA, California, Iran, Greece and Turkey. The detailed information about the individual events used to obtain the I_{100} values is listed in Table 3. Each region is identified with a different symbol in Fig. 11. The magnitudes of great Indian earthquakes are taken from the recent catalogue of Abe (1981). One can see clear evidence of high values of intensity (I_{100}) for eastern Himalayas events and for the not very distant Bihar Nepal event. Three out of the five events of the group show values of I_{100} above the CNEA average, and two are above the $+1\sigma$ line. The trend of Johnston (1996b) is

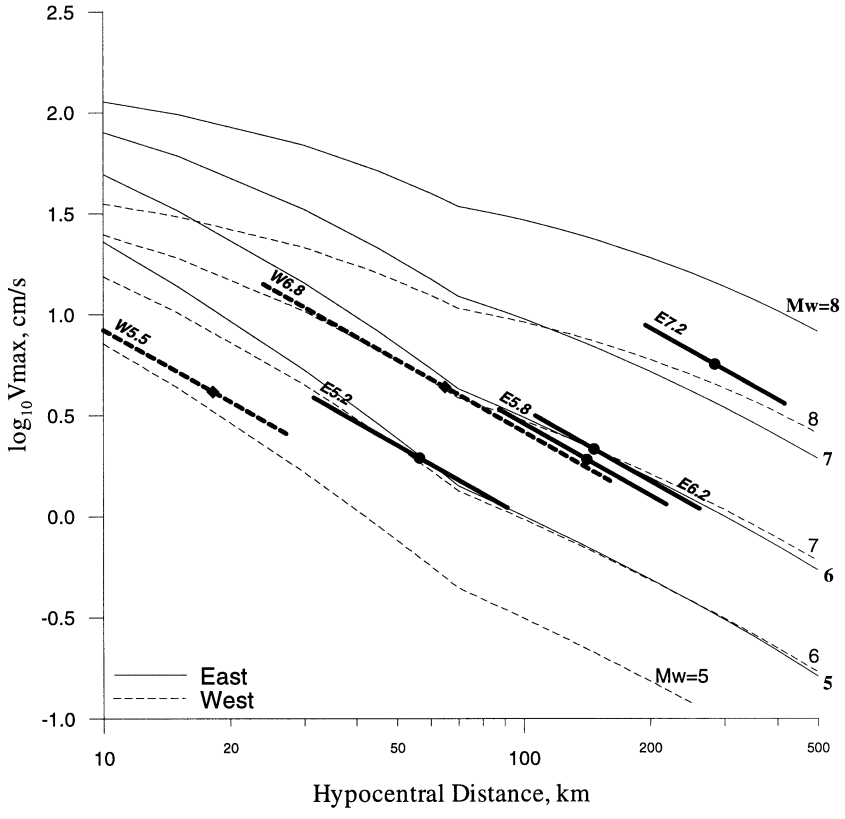

Figure 9. Same as Fig. 6(a) but for $\log_{10}$ peak velocity.

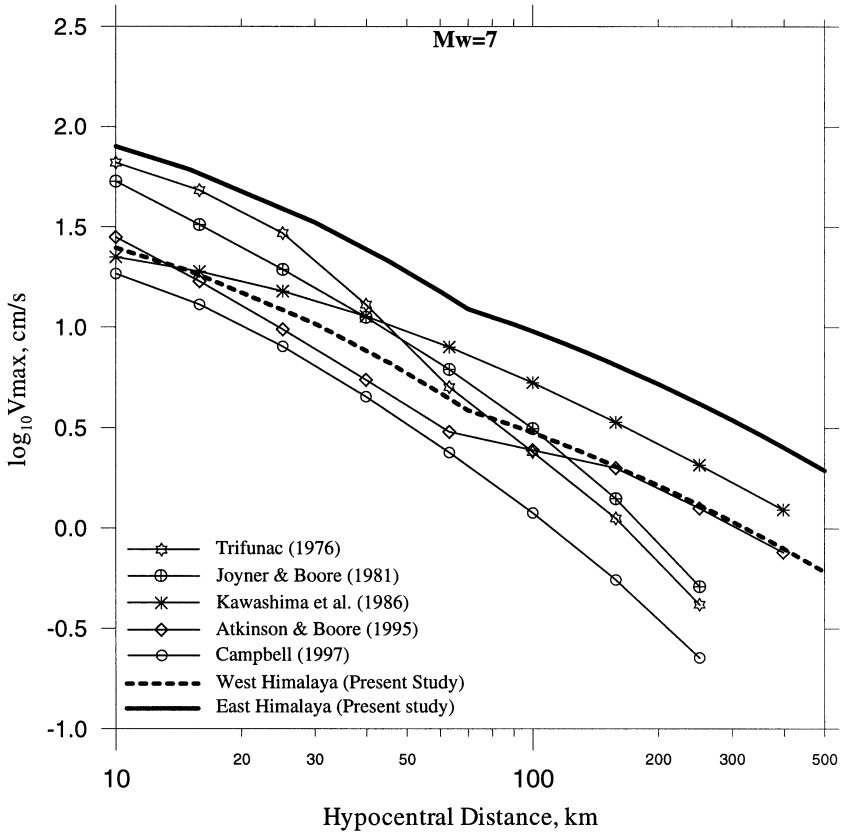

Figure 10. Comparison of our results for expected $\log_{10}$ peak velocity versus hypocentral distance with those of other authors. Our results are shown as a thick solid line for the eastern Himalayas and a thick dashed line for the western Himalayas for $M_w = 7$. The thin curves with open symbols are from different authors for different regions of the world.

Table 3. List of events used as macroseismic evidence.

No.	Date	Latitude	Longitude	Magnitude	I_0*	I_{100}†	Ref.§
Eastern Himalayas							A
1	1897 June 12	25.9°N	91.8°E	8.7	12.27	10.32	
2	1918 July 8	24.5°N	91.0°E	7.6	8.78	6.83	
3	1930 July 2	25.5°N	90.0°E	7.1	9.05	7.10	
4	1950 August 15	28.5°N	96.7°E	8.6	11.29	9.34	
Western Himalayas							A
5	1905 April 4	32.7°N	76.3°E	8.1	9.74	7.26	
6	1975 January 19	32.5°N	78.4°E	6.8	8.98	6.45	
7	1991 October 19	30.78°N	78.77°E	7.0	8.50	6.31	
Bihar–Nepal							A
8	1934 January 15	26.3°N	86.0°E	8.3	11.03	8.74	
Peninsular India							A
9	1900 February 8	10.8°N	76.8°E	6.0	9.34	6.15	
10	1938 March 14	21.5°N	75.8°E	6.3	10.11	6.92	
11	1956 July 21	23.0°N	70.0°E	6.1	8.78	5.59	
12	1967 December 10	17.7°N	73.9°E	6.0	9.23	6.04	
Central United States (New Madrid)							B
13	1811 December 16	36.6°N	89.6°W	8.0	11.81	9.22	
California (San Andreas)							B
14	1952 July 21	35.0°N	119.0°W	7.7	9.97	6.64	
Iran							C
15	1811 September 1	36.6°N	49.8°E	7.25	9.39	5.41	
16	1968 August 31	34.0°N	59.0°E	7.3	8.93	4.95	
17	1972 April 10	28.4°N	52.8°E	7.1	8.92	4.93	
18	1977 March 21	27.6°N	56.4°E	7.0	8.76	4.77	
Greece							D
19	1981 February 24	38.1°N	22.9°E	6.8	8.60	5.22	
20	1981 February 25	38.1°N	23.1°E	6.4	8.50	5.12	
21	1981 March 4	38.13°N	23.2°E	6.4	9.00	5.63	

* Derived epicentral M.M. Intensity originally cited by different authors.
† Intensity at a distance of 100 km calculated in this paper using the original I_0 values and the regionally specific version of the attenuation formula.
§ A: Chandra (1980) except event no. 7
B: Chandra (1979)
C: Chandra *et al.* (1979)
D: Tilford *et al.* (1985)

about 1.5 grades of I_{100} above the line for 'tectonic' regions of CNEA and somewhat overpredicts, if extrapolated, the eastern Himalayas observations. This indicates that the East Himalayan earthquake sources and the earthquake population studied by Johnston may have some common properties. Of the three data points representing the western Himalayas, one is around $+1\sigma$, another is near the average and the last is near -1σ. This amount of data is too small for a decisive judgement, but suggests regular or low values of I_{100} for this region. Most of the data for the other regions, viewed as a whole, agree reasonably well with the CNEA trend. Two very pronounced anomalies are the 1811 New Madrid series, treated as a single event, and the Peninsular India group. These sources are located within the old continental crust, and this kind of geological background may provide at least a partial explanation for the anomalous eastern Himalayas data. On the whole, the anomalous character of strong-motion amplitudes in the eastern Himalayas is confirmed fairly reliably by the macroseismic data, whereas there is no indication of anomalies for the western Himalayas.

The macroseismic data for the Himalayan earthquakes are indicative of specific, relatively gradual distance decay (Chandra 1979, 1980; Gupta & Trifunac 1988). This fact is in good agreement with the behaviour of the attenuation of peak accelerations revealed in the present study (Fig. 7). Following Gupta & Trifunac (1988), but with wider evidence, we may conclude that in terms of the shape of the attenuation curve, the decay of accelerations, velocities and intensities in eastern USA represents the best-published analogy to the east Himalayan data.

8 DISCUSSION

To establish regional attenuation relationships for peak ground acceleration and velocity is an important practical issue. With a limited amount of data, in the present study we could obtain no more than tentative conclusions about the behaviour of strong ground motion amplitudes in the Himalayan region. Previous studies of this kind by Chandrasekaran (1994), Singh *et al.*

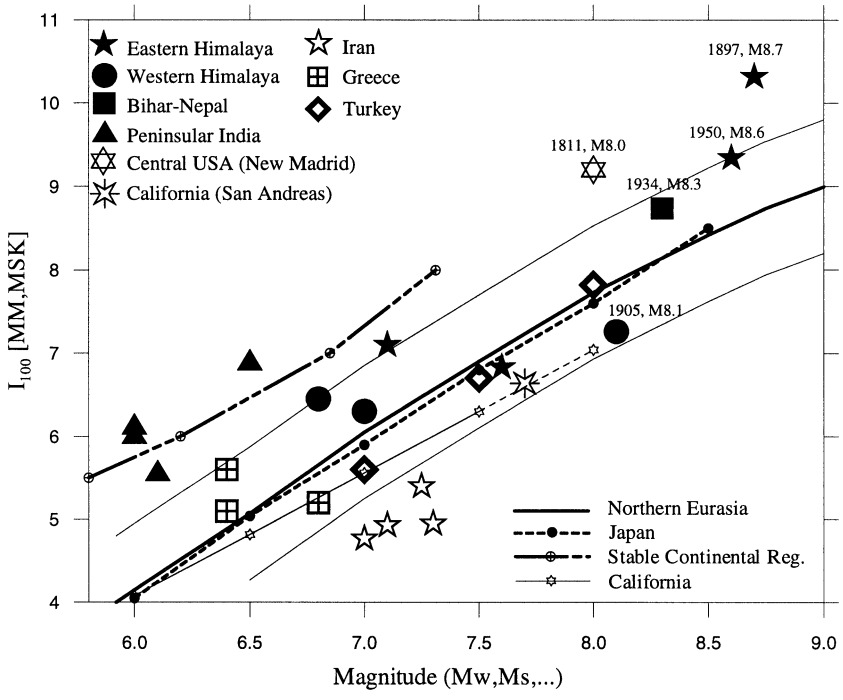

Figure 11. Intensity values at 100 km (I_{100}) versus magnitude for a number of events in India and other parts of the world. The thick continuous line is the reference curve for continental northern Eurasia (CNEA) and the thin continuous lines are its $\pm 1\sigma$ bounds. The thick dashed line is the curve for the Japanese region from Gusev & Shumilina (2000) and the thick dot-dashed line is for the stable continental region from Johnston (1996b).

(1996) and Sharma (1998) give empirical generalizations of the attenuation of peak acceleration with distance for the Himalayas, but, as one can see from the results of this study, further steps in the data analysis are quite justified. The most important outcome of the present study is the zonation of the Himalayan region into the eastern and western Himalayas. We believe that the application of the analysis to a very inhomogeneous data set as done by the authors mentioned above is the cause of the very unusual average relationships that they obtained. It is seen in Fig. 7 that the distance decays for acceleration given by Singh *et al.* (1996) and Sharma (1998) are much more gradual than the other published curves, whereas Chandrasekaran (1994) predicts amplitudes that are probably too high in the vicinity of the source. (Similarly, too gradual attenuation was found by Singh *et al.* 1996 for the velocity.)

The use of theoretical amplitude curves may be criticized on account of the possible differences between the assumed and the real shapes of the acceleration spectra. We have analysed, in a preliminary manner, the Fourier spectra of acceleration for our data and found these shapes quite standard, reminiscent of the Californian and Japanese shapes that were the basis for Gusev's (1983) spectral scaling. Thus, the 'theoretical' distance dependence of $A_{\max}$ may be expected to be relatively reliable. On the other hand, the prediction of magnitude dependence of $A_{\max}$ (on the basis of spectral scaling laws, e.g. those of Brune 1970 and Gusev 1983), is less reliable (*cf.* Singh *et al.* 1989), hence the empirical trend proposed by Fukushima & Tanaka (1990) has been used. We wish to emphasize that we adopt a reliable empirical shape from a well-studied region and that it corresponds to a very well-studied distance range. In our view, this approach is the most reliable one when one needs to predict the magnitude dependence in a region with a small amount of data.

Another possible cause of error in our attenuation curves is the particular definition of the source-related duration used in the SSK program, which is based on the whole-source rupture propagation time (see the description of the algorithm in the Appendix). This assumption seems to be acceptable at hypocentral distances comparable to the source size, but at very small distances from the fault the source-related component of the duration may become significantly smaller than the total source-process or rupture duration. As path-related duration is negligible here, a significant overestimation of the total duration, and thus an underestimation of the amplitude, may result. How large may this underestimation be? To find the answer theoretically requires the determination of too many unknowns. Resorting to an empirical approach one may note that the observed values of the horizontal peak acceleration in the epicentral areas of many earthquakes often do not show significant amplification very near to the causative fault. Also, macroseismic data usually show plain gradual saturation of intensity at intermediate to very near distances from the fault. Thus, the underestimation of the mean amplitudes by the present version of SSK in the vicinity of the fault may hardly be more than 1.5–2 times. On the other hand, our mode of predicting the Fourier spectral level is much more robust, and may be appropriate even 5–15 km from the fault surface. Hence, at most distances (large, comparable to source size or even somewhat smaller), our expected peak accelerations (Fig. 6a) may be safely considered as realistic estimates of mean amplitudes. At distances much smaller than the source size, however, these estimates should be treated rather as lower bound estimates, and somewhat underestimate peak amplitudes in the vicinity of the fault, but by hardly much more than 1.5–2 times.

An important issue is the geophysical or tectonophysical cause of unusually high accelerations, velocities and I_{100} for the

eastern Himalayas. One possibility is the common site effect specific for all stations of the Shillong array but geological data do not provide support for this idea. Nevertheless, some contribution of the site effects (common to the entire network) to the observed 300 per cent increase of amplitudes cannot be excluded, but we have no access to site geology data. An implicit hint that site effects can hardly be large is the small site-related variance of amplitudes, but this kind of argument is far from being convincing. The relatively small contribution of the site effects to the total scatter of the Himalayas data is in prominent contrast to similar analyses applied to Kamchatka strong-motion data (Gusev & Petukhin 1995, 1996), where the contribution from the station terms is large or even dominating, whereas subregion effects are difficult to observe (although quite possible).

In the search for an explanation of the anomalous amplitudes we consider the possible effect of an unusual anomalous spectral shape. This possibility has been checked by direct inspection, and it has been rejected because the spectral shapes are of quite common appearance. Moreover, the mere fact that an anomaly of comparable amplitude is present both for acceleration and velocity indicates that unusual spectral shapes can hardly be an explanation. The actual anomaly is related not to the spectral shape but rather to its level. Hypothetically, such kinds of anomalies may be associated with high stress drops of the relevant earthquake faults. The high values of I_{100} common to the eastern Himalayas and to the Peninsular India events favour this possibility. Such a coincidence probably indicates some specific property of old, continental crust, in agreement with Müller (1978) and Panza (1980) and also with the study of Johnston (1996a) on the earthquakes of stable continental regions. The finding that I_{100} levels of eastern Himalayas events are only somewhat below those expected for 'stable continental' events (Fig. 10) means that eastern Himalayan events are intrinsically intraplate events. Their location in the vicinity of the first-order plate boundary should be better specified as 'active continental region' in terms of Johnston (1996a), and the I_{100} levels fit this idea. Meanwhile, the analogy between $A_{\max}$ levels of the western Himalayas events and Japanese data may be interpreted as the analogy between stress and strength conditions in usual subduction zones and in the Himalayan main thrust fault.

We believe, tentatively, that the property of the subregion relevant to observed anomalies is mean fault strength, directly manifested in the stress drop value. The critical check for this hypothesis is its capability to explain why the phenomenon is specific to the eastern Himalayas and not the western Himalayas. We find the explanation in the fact that the events from the western Himalayas are shallower ones, so that their causative faults are within the roots of high mountain ranges that essentially represent the giant tectonic slivers of the accretionary wedge, highly deformed, fluid-saturated and probably of relatively moderate to low strength. The hypocentres of the events in the eastern Himalayas, however, are deeper (all below 25 km depth) and their causative faults are within the relatively drier and higher-strength shield crust. This explanation is far from being final, but may well be of relevance.

We may become more confident in the proposed explanation if it agrees with the observed character of the distance attenuation of amplitudes. Indeed, we see anomalously low attenuation that is common to both subregions, and this feature may well be related to the same shield crust that is cold, low scattering and has a high Q factor. For the eastern Himalayas, both sources and receivers are located in such a structure, so its effect is immediate, whereas for the western Himalayas, diving seismic rays (characteristic of epicentral distances above 70 km) must first propagate for some distance through the 'tectonic' low-Q accretionary crust and only after crossing the interplate boundary dive into the subducted shield crust where they propagate for most of the whole path to the receivers. Near the receivers, a short segment of low-Q path may occur again, but this amount cannot change the increased value of the ray-averaged, whole-path Q. Qualitatively similar effects might be expected if the wave propagation is treated as a surface wave phenomenon. Therefore, the gross net effect of an unusually low attenuation may be expected to be comparable for both subregions.

We have not used the existing strong-motion records from Peninsular India in our study, but their use for further research may be helpful, in particular to find out whether they agree with the macroseismic anomaly observed in that region.

To put our results, which indicate probable high accelerations in the epicentral zones of the eastern Himalayas, in a broader context, we describe the effects of the great Assam earthquake of magnitude 8.7 that occurred in 1897. This unique event, with intensity levels from X to XII (MCS) throughout the entire epicentral area of about 150×80 km^2, occurred in the eastern Himalayas. In his classic text, Richter (1958) quoted the impressive field report by Oldham (1899) about this event. One of the most unusual observations was that of many large boulders thrown up and out of the ground without damaging the rims of their former seats. This high acceleration is consistent with evidence in the granite rock of Assam Hills of widespread surface distortion and complex fracturing best characterized as shattering. Richter noted that Oldham's description of the epicentral area of the 1897 event was actually the model case for compiling a description of grade XII of the scale.

9 CONCLUSIONS

In the strong-motion data analysis, instead of empirical formulae we use a theoretical magnitude-dependent distance attenuation in the data reduction for distance, and an empirical acceleration versus magnitude trend, from a well-studied region, in the data reduction for magnitude. This approach is applicable to rather limited data sets with insufficient distance–magnitude coverage and it permits us to establish conservatively the shape and level of $A_{\max}(M_w, R)$ and $V_{\max}(M_w, R)$ relationships applicable to the Himalayas.

The pronounced inhomogeneity of the observed data is ascribed to differences between the two subregions of the eastern and western Himalayas. Of these, the western Himalayas region is comparable, in terms of near-source amplitudes, to the Japan region, whereas the amplitudes in the eastern Himalayas are three times larger, and have no direct analogue amongst the other seismic regions of the Earth that have been studied in detail. We believe that horizontal epicentral accelerations in excess of 1–1.5 g are typical here.

Using strong-motion records, the difference between these two subregions can be established only on the basis of a very limited number of events and thus it is not completely reliable; however, a similar difference can be found in macroseismic data, making the identification of the two subregions definite. The Great 1897 Assam earthquake is a particular prominent example of an unusual, uniquely powerful eastern Himalayas event.

This peculiarity may be related to the fact that the sources of the eastern group are deep-seated in relatively undisturbed old continental lithosphere of probably high strength, whereas the western Himalayas sources are nearer to the surface and surrounded by highly dislocated accretionary complexes, with relatively low strength, similar in their properties to usual tectonic environments. The rather slow attenuation with distance of strong-motion amplitudes and of the macroseismic intensity indicates the presence of a high-frequency crustal waveguide with very low attenuation. This feature seems to be common to both subregions.

An important conclusion of our study is that the combined use of instrumental and macroseismic data is a powerful tool for the detailed analysis of seismic hazard. It permitted us to check the conclusions based essentially on an insufficient amount of data and to validate them by independent observations. The presence of unusually high typical amplitudes in the eastern Himalayas and also the slow distance decay for the entire Himalayas should be incorporated into future seismic hazard assessments for this region.

ACKNOWLEDGMENTS

We thank the Department of Science and Technology, Government of India, for making available the strong-motion data. Constructive comments from Prof. M. D. Trifunac and an anonymous reviewer were helpful in improving the quality of the paper. Eugenia Guseva performed the spectral analysis of the accelerograms. IAP is thankful to Prof. G. Furlan, Head, Training and Research in Italian Laboratory (TRIL) program of ICTP for providing a grant. Financial support from CNR GNDT (contract 98.3238.PF54) is also acknowledged. AAG acknowledges support from the Russian Foundation for Basic Research (project 97–05–65056).

REFERENCES

Abe, K., 1981. Magnitude of large shallow earthquakes from 1904 to 1980, *Phys. Earth planet. Inter.,* **27,** 72–92.

Ambraseys, N.N., 1995. The prediction of earthquake peak ground acceleration in Europe, *Earthq. Eng. Struct. Dyn.*, **24,** 467–490.

Atkinson, G.M. & Boore, D.M., 1995. Ground-motion relations for eastern North America, *Bull. seism. Soc. Am.,* **85,** 17–30.

Boore, D.M., 1983. Stochastic simulation of high-frequency ground motions based on seismological models of the radiated spectra, *Bull. seism. Soc. Am.,* **73,** 1865–1894.

Brune, J.N., 1970. Tectonic stress and the spectra of seismic shear waves from earthquakes, *J. geophys. Res.,* **75,** 4997–5009.

Campbell, K.W., 1997. Empirical near-source attenuation relationships for horizontal and vertical components of peak ground acceleration, peak ground velocity, and pseudo-absolute acceleration response spectra, *Seism. Res. Lett.,* **68,** 154–179.

Chandra, U., McWhorter, J.G. & Nowroozi, A.M., 1979. Attenuation of intensities in Iran, *Bull. seism. Soc. Am.,* **69,** 237–250.

Chandra, U., 1979. Attenuation of intensities in the United States, *Bull. seism. Soc. Am.,* **69,** 2003–2024.

Chandra, U., 1980. Attenuation of intensities in India, *Proc. 7th WCEE*, Vol. 2, pp. 521–524, Istanbul, Turkey.

Chandrasekaran, A.R., 1994. Evaluation of design earthquake parameters for a site and utilization of strong motion data, *Current Sci.,* **67,** 353–358.

Chandrasekaran, A.R. & Das, J.D., 1992. Strong motion arrays in India and analysis of data from Shillong array, *Current Sci.,* **62,** 233–250.

Chen, W.P. & Molnar, P., 1990. Source parameters of earthquakes and intraplate deformation beneath the Shillong plateau and the northern Indoburman ranges, *J. geophys. Res.,* **95,** 12 527–12 552.

Erdik, M., Doyuran, V., Akkas, N. & Gulkan, P., 1985. A probabilistic assessment of seismic hazard in Turkey, *Tectonophysics,* **117,** 295–344.

Evans, P., 1964. The tectonic framework of Assam, *J. geol. Soc. India,* **5,** 80–96.

Fukushima, Y. & Tanaka, T., 1990. A new attenuation relation for peak horizontal acceleration of strong earthquake ground motion in Japan, *Bull. seism. Soc. Am.,* **80,** 757–783.

Gansser, A., 1964. *Geology of the Himalayas,* Interscience, New York.

Gansser, A., 1977. The great suture zone between Himalaya and Tibet: a preliminary account, in *Himalaya: Sciences de la Terre,* pp. 181–192, ed. Jest, C. Colloq., Int. CNRS, 268, Ecologie et geologie del'Himalaya, Paris.

Gupta, I.D. & Trifunac, M.D., 1988. Attenuation of intensity with epicentral distance in India, *Soil Dyn. Earthq. Eng.,* **7,** 162–169.

Gusev, A.A., 1983. Descriptive statistical model of earthquake source radiation and its application to an estimation of short-period strong motion, *Geophys. J. R. astr. Soc.,* **74,** 787–808.

Gusev, A.A., 1991. Intermagnitude relationsips and asperity statistics, *Pure appl. Geophys.,* **136,** 515–527.

Gusev, A.A., 1996. Peak factors of Mexican accelerograms: evidence of non-Gaussian amplitude distribution, *J. geophys. Res.,* **101,** 20 083–20 090.

Gusev, A.A. & Pavlov, V.M., 1991. Deconvolution of squared velocity waveform as applied to study of non-coherent short-period radiator in earthquake source, *Pure appl. Geophys.,* **136,** 235–244.

Gusev, A.A. & Petukhin, A.G., 1995. An algorithm for forcasting parameters of earthquake ground motion, *Vulk. Seism.,* **4–5,** 182–192 (in Russian).

Gusev, A.A. & Petukhin, A.G., 1996. Methods for constructing of regional relationships among the parameters of seismic ground motions, magnitude and distance with limited data: example of Kamchatka maximum accelerations, *Bulgarian geophys. J.,* **22,** 40–49.

Gusev, A.A. & Shumilina, S., 2000. Modelling the intensity–magnitude–distance relation based on the concept of an incoherent extended earthquake source, *Volc. Seism.,* **21,** 443–463.

Gusev, A.A., Gordeev, E.I., Guseva, E.M., Petukhin, A.G. & Chebrov, V.N., 1997. The first version of the A_{max}(Mw, R) relationship for Kamchatka, *Pure appl. Geophys.,* **149,** 299–312.

Hudson, D.E., Trifunac, M.D., Brady, A.G. & Vijayaraghwan, A., 1971. Strong motion earthquake accelerograms, ii, corrected acceleration and integrated velocity and displacement curves, *Earthquake Engineering Research Laboratory, EERL,* 71–50, California Institute of Technology, Pasadena.

Johnston, A.C., 1996a. Seismic moment assessment of earthquakes in stable continental regions—I. Instrumental seismicity, *Geophys. J. Int.,* **124,** 381–414.

Johnston, A.C., 1996b. Seismic moment assessment of earthquakes in stable continental regions—II. Historical seismicity, *Geophys. J. Int.,* **125,** 639–678.

Joyner, W.B., 1984. A scaling law for the spectra of large earthquakes, *Bull. seism. Soc. Am.,* **74,** 1167–1188.

Joyner, W.B. & Boore, D.M., 1981. Peak horizontal acceleration and velocity from strong-motion records including records from the 1979 Imperial Valley, California, earthquake, *Bull. seism. Soc. Am.,* **71,** 2011–2038.

Joyner, W.B. & Boore, D.M., 1993. Methods for regression analysis of strong-motion data, *Bull. seism. Soc. Am.,* **83,** 469–487.

Kaila, K.L. & Sarkar, D., 1977. Earthquake intensity attenuation pattern in India, *Proc. Symp. Analysis of Seismicity and Seismic Risk,* 173–191, Liblice, Czechoslovakia.

Kanamori, H. & Anderson, D.L., 1975. Theoretical basis of some empirical relations in seismology, *Bull. seism. Soc. Am.,* **65,** 1073–1095.

Kawashima, K., Aizawa, K. & Takahashi, K., 1986. Attenuation of peak ground acceleration, velocity and displacement based on multiple regression analysis of Japanese strong motion records, *Earthq. Eng. Struct. Dyn.,* **14,** 199–215.
Kawasumi, H., 1951. Measures of earthquake danger and expectancy of intensity throughout Japan as inferred from the seismic activity in historical times, *Bull. Earthq. Res. Inst.,* **29,** 469–482.
Khattri, K.N., Rogers, A.M., Perkins, D.M. & Algermissen, S.T., 1984. A seismic hazard map of India and adjacent areas, *Tectonophysics,* **108,** 93–134.
Lee, V.W. & Trifunac, M.D., 1979. *Automatic Digitization and Processing of Strong Motion Accelerograms, Part II, Computer Processing of Accelerograms,* Rept 79–15 II, Dept Civil Engineering, University of Southern California, Los Angeles.
Lee, V.W. & Trifunac, M.D., 1985. *Attenuation of Modified Mercalli Intensity for Small Epicentral Distance in California,* Rept CE 85–01, Dept Civil Engineering, University of Southern California, Los Angeles.
LeFort, P., 1975. Himalayas: the collided range. Present knowledge of the continental arc, *Am., J. Sci.,* **275A,** 1–44.
Mitchell, A.H.G., 1981. Phanerozoic plate boundaries in mainland SE Asia, the Himalaya and Tibet, *J. geol. Soc. Lond.,* **138,** 109–122.
Morse, P.M. & Feshbach, H., 1953. *Methods of Theoretical Physics,* McGraw-Hill, New York.
Müller, St., 1978. The evolution of the earth crust, in *Tectonics and Geophysics of Continental Rifts,* pp. 11–28, eds Ramberg, I.B. & Neuman, E.R., Reidel, Dordrecht.
Ni, J. & Barazangi, M., 1984. Seismotectonics of the Himalayan collision zone: geometry of the underthrusting Indian plate beneath the Himalaya, *J. geophys. Res.,* **89,** 1147–1163.
Ohno, S., Ohta, T., Ikerua, T. & Takemura, M., 1993. Revision of attenuation formula considering the effect of fault size to evaluate strong-motion spectra in near field, *Tectonophysics,* **218,** 69–81.
Oldham, H.D., 1899. Report on the great earthquake of June 12, 1897, *Mem. geol. Surv. India,* **29,** 1–379.
Panza, G.F., 1980. Evolution of the Earth's lithosphere, in *Mechanisms of Continental Drift and Plate Tectonics,* pp. 75–87, eds Davies, P.A. & Runcorn, S.K., Academic Press, London.
Rautian, T.G., Khalturin, V.I., Dotsev, N.T. & Sarkisyan, N.M., 1989. Macroseismic magnitude, *Voprosy Inzhenernoy Seismologii,* 30, 98–109, Nauka, Moscow (in Russian).
Richter, C.F., 1958. *Elementary Seismology,* Freeman, San Francisco.
Sabetta, F. & Pugliese, A., 1987. Attenuation of peak horizontal acceleration and velocity from Italian strong-motion records, *Bull. seism. Soc. Am.,* **77,** 1491–1513.
Sharma, M.L., 1998. Attenuation relationship for estimation of peak ground horizontal acceleration using data from strong-motion arrays in India, *Bull. seism. Soc. Am.,* **88,** 1063–1069.
Singh, R.P., Aman, A. & Prasad, Y.J.J., 1996. Attenuation relations for strong seismic ground motion in the Himalayan region, *Pure appl. Geophys.,* **147,** 161–180.
Singh, S.K., Ordaz, M., Anderson, J.G., Rodriguez, M., Quaas, R., Mena, E., Ottaviani, M. & Almora, D., 1989. Analysis of near source strong-motion recordings along the Mexican subduction zone, *Bull. seism. Soc. Am.,* **79,** 1697–1717.
Sinha-Roy, S., 1982. Himalaya Main Central Thrust and its implications for Himalayan inverted metamorphism, *Tectonophysics,* **84,** 197–224.
Street, R.L. & Turcotte, F.T., 1977. A study of northeastern North American spectral moments, magnitudes and intensities, *Bull. seism. Soc. Am.,* **67,** 599–614.
Tilford, N.R., Chandra, U., Amick, D.C., Moran, R. & Snider, F., 1985. Attenuation of intensities and effect of local site conditions on observed intensities during the Corinth, Greece, earthquakes of 24 and 25 February and 4 March 1981, *Bull. seism. Soc. Am.,* **75,** 923–937.
Trifunac, M.D., 1976. Analysis of the peaks of strong earthquake ground motion—dependence of peaks on earthquake magnitude, epicentral distance, and recording site conditions, *Bull. seism. Soc. Am.,* **66,** 189–219.
Trifunac, M.D. & Brady, A.G., 1975. A study of the duration of strong earthquake ground motion, *Bull. seism. Soc. Am.,* **65,** 581–626.
Trifunac, M.D. & Lee, V.W., 1990. Frequency dependent attenuation of strong earthquake ground motion, *Soil Dyn. Earthq. Eng.,* **9,** 3–15.
Valdiya, K.S., 1980. The two intracrustal boundary thrusts of the Himalaya, *Tectonophysics,* **66,** 323–348.
Wadia, D.N., 1975. *Geology of India,* Tata McGraw-Hill, New Delhi.

APPENDIX A: SHORT DESCRIPTION OF THE ALGORITHM OF THE SSK CODE FOR ESTIMATING HIGH-FREQUENCY STRONG-MOTION AMPLITUDES

The SSK code (for the initial version see Gusev & Petukhin 1995, 1996) has been written for the approximate evaluation of high-frequency seismic strong-motion amplitudes (as well as duration and spectra). It has been designed for practical use in engineering seismology, to meet the need for a technique for the fast simplified forecasting of median parameters of strong ground motion related to a specific earthquake source, wave propagation path and site. The SSK algorithm reproduces the approach of Gusev (1983) very closely.

A1 General outline of the algorithm

The flow chart in Fig. A1 illustrates the principal relations between the initial, intermediate and output quantities of the algorithm. The main input parameters are the moment magnitude M_w [or seismic moment M_0; $\log_{10}M_0 = 1.5(M_w + 10.7)$] and the hypocentral distance R. The properties of an event of a given M_w from a particular seismic zone are described by the 'source acceleration spectrum', $K(f) = f^2|\dot{M}_0(f)|$ (Gusev 1983), where $\dot{M}_0(f)$ is the Fourier spectrum of the seismic moment rate of an equivalent point dipole. From the $K(f)$ spectrum, taking into account the geometrical spreading, loss, etc., we determine the Fourier acceleration spectrum $FS(f)$ for the bedrock, which is the first main intermediate parameter of the algorithm. The distance attenuation function used combines the point source attenuation and the saturation effect of a finite source. The second main characteristic, the total signal duration T_{total}, is found by combining the source (rupture) duration and the duration component determined by the medium (path).

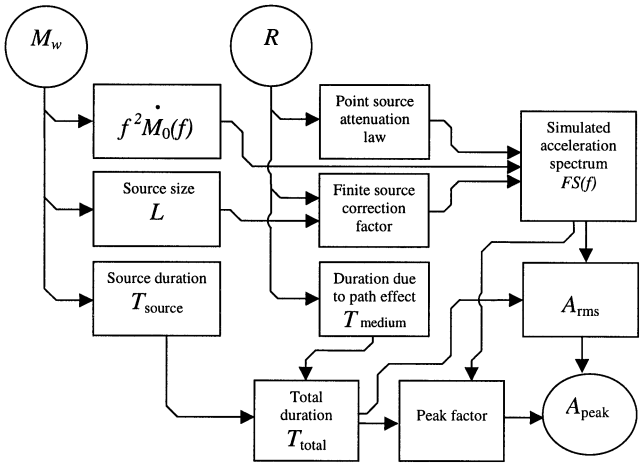

Figure A1. Diagram of the algorithm used in the Appendix.

Given the Fourier spectrum and the duration, another ground motion parameter can easily be evaluated using random vibration theory (Gusev 1983; Boore 1983).

A2 Specifying the basic reference spectrum

The acceleration source spectrum $K(f)$ is defined by the 'spectrum scaling law' function $K(f, M_0)$. This function is either tabulated or defined by an analytical formula. By default, we use the $K(f, M_0)$ table based on Gusev (1983). This semi-empirical scaling law was derived by fitting observational data of many kinds using the hypothesis of source similarity only for the lower-frequency part of the spectrum (around the corner frequency). It can be considered as a good starting approximation for applications in engineering seismology. As a standard analytical model, the Brune (1970) spectral model is used with the modification of Joyner (1984) with four parameters: M_0, stress drop $\Delta\sigma$, corner frequency f_c and acceleration upper spectral cut-off frequency f_{max}. To account for the vertical impedance gradient, spectral corrections are added to the source spectrum. Alternatively, the reference median smoothed $FS(f)$ spectrum for a fixed (M_w, R) combination may be specified in tabular form (based for example on observations in the target area) to be further extrapolated to other M_w and R values.

A3 Point-source spectral amplitude attenuation

We assume that the geometrical spreading can be described as two hyperbolic branches: *a* ('body wave') and *b* ('surface wave') with an intersection at $R=R_c$ (Street & Turcotte 1977). Thus, the point-source attenuation law for $FS(f)$ has the form

$$G(R,f)=\begin{cases} g_1(R, Q_a(f)); & R<R_c \\ C(f)g_{0.5}(R, Q_b(f)); & R>R_c \end{cases},$$

where $g_n(R, Q) = R^{-n}\exp(-\pi fR/cQ)$, $C(f) = g_1(R_c, Q_a(f))/g_{0.5}(R_c, Q_b(f))$, and c and $Q_{a,b}(f)$ are the S-wave velocity and frequency-dependent quality factor, respectively. We assume $Q(f)=Q_0 f^{\gamma}$ if $f>f_0=1$ Hz, and $Q(f)=Q_0$ otherwise.

A4 Specifying the scaling of source parameters

The rupture duration, T, and the source length, L, are important quantities in the calculation. They are determined from M_w based on the concept of the approximate geometric and kinematic similarity of earthquake sources (Kanamori & Anderson 1975). Both T and L are assumed to grow as the cubic root of the seismic moment. In particular, we assume $\log_{10}L = 0.5M_w - 1.85 + \in$, where $\in = \delta \mathrm{Log}_{10}L$ represents a correction describing the deviation of the stress drop from its typical value. To compute the rupture duration we then assume that $L=vT$, where the default value is $v=3.5$ km s^{-1}.

A5 Amplitude saturation near an extended source

The Fourier acceleration spectrum at a recording point that is close to the surface of a finite source may be significantly lower than that at the same distance from a point source with the same $K(f)$ spectrum because a large part of the radiating surface is far from the receiver. In order to describe formally such saturation effects, Gusev (1983) developed a simple theory for the wavefield around an incoherently radiating surficial source. For a disc-shaped source, he derived a simple approximate formula,

$$\left(\frac{FS}{FS_{\text{point source}}}\right)^2 = \frac{R^2}{R_s^2}\log_e\left(\frac{R^2+R_s^2}{R^2+R_{coh}}\right),$$

where R_s is the source radius, R is the hypocentral distance and R_{coh} is the coherence radius of the source (taken as 1 km). This formula is applicable to spectral amplitudes at all sufficiently high frequencies when the source radiation can be treated as an incoherent (noise-like, random) signal. The formula was originally proposed for rms amplitudes, but it is directly applicable to spectral amplitudes using Parseval's theorem (Morse & Feshbach 1953). For practical use, we replace R_s by the effective source radius R_{eff}, defined as $(S/\pi)^{0.5}$, where $S=LW$ is the source area. The formula was successfully tested against real earthquake data by Trifunac & Lee (1990), who compared it to three other formulae and found it superior in describing the near-source effects contained in the western USA accelerograms set, and by Ohno *et al.* (1993), who performed a more detailed check against near-source data of two well-recorded earthquakes. Recently, the SSK program was supplemented by an alternative, more accurate procedure to calculate the near-source saturation effect using the numerical integration of the contributions from a rectangular source of arbitrary aspect ratio (see Gusev & Shumilina 2000 for details). For all but extremely elongated sources, the resulting adjustments (averaged over azimuth) are minor.

A6 Incorporation of soil conditions

The effects of site geology are taken into account by SSK only in a rudimentary manner: for intermediate and soft ground categories, spectral corrections are tabulated with respect to the bedrock, taken as a reference. These corrections are amplitude-independent; however, to account primitively for the non-linear enhancement of attenuation in soil, the applied corrections correspond to a significant amplitude level (peak acceleration 0.1–0.2 g on bedrock); therefore, the ground layer is treated as a simple equivalent-linear element.

A7 Calculation of the Fourier spectrum

The Fourier spectrum for fixed M_w and R is computed from $K(f, M_0(M_w))$, applying all relevant factors that account for impedance ratio, mean S-wave radiation pattern, partition into vectorial components, free-surface effect, geometric spreading, loss (Q-factor), finite-source effect and ground-type/site correction.

A8 Calculation of duration

We believe that the accelerogram duration can be estimated by combining source/rupture-related duration and the path-related duration. Sometimes, site-related duration is also important, in particular for non-rock ground, but SSK ignores this possibility. The path-related broadening of the *S*/*Lg*-wave group, observed most frequently in records of small to moderate earthquakes with short source duration for frequencies above 1 Hz is a complex phenomenon that can be treated as a

combined effect of forward scattering, dispersion, wave conversion and multiray propagation. We incorporate this effect on an empirical basis. Following Trifunac & Brady (1975), we describe this effect as a linear increase of duration with distance: $T_{\text{medium}} = T_1(R/R_1)$, where T_1 is an empirical constant that depends on the region and also on the definition of duration, and R_1 is a fixed reference distance, normally taken as 100 km.

In order to combine source and path contributions to the duration we use the formal approach (see Gusev 1983; Gusev & Pavlov 1991) based on the assumption that the time history function for mean squared amplitude (MSA) of the recorded incoherent wave group may be considered as a convolution of the MSA function of the wave pulse radiated by the source and of the MSA function that represents the pulse response of the medium (empirical Green's function for MSA). With this assumption, we immediately find that the second central moment, or mean square duration (MSD), of a squared record is the sum of the MSD values of the two component functions (source and medium components):

$$T_{\text{rms}}^2 = T_{\text{rms,s}}^2 + T_{\text{rms,m}}^2 ,$$

where

$$T_{\text{rms}}^2 = \frac{e_2}{e_0} - \left(\frac{e_1}{e_0}\right)^2 ,$$

$$e_k = \int_0^\infty t^k A_{\text{MSA}}(t)^2 dt , \quad (k = 0, 1, 2) .$$

Using this approach in practice we first convert, for each component, the usual definitions of duration to $\text{MSD} = T_{\text{rms}}^2$, and after summation, we convert the combined MSD or T_{rms} to the effective duration T_{eff}, which is a measure of duration relevant to our aims. We define T_{eff} for an arbitrary finite-duration signal as the duration of a signal with a boxcar envelope (that is, a segment of a stationary noise) that has the same total energy and same rms amplitude as the total energy of the reference signal and the rms amplitude of the reference signal in the vicinity of its maximum. Usually, $T_{\text{eff}} = (1.5\text{–}3)T_{\text{rms}}$; in SSK the default setting is $T_{\text{eff}} = 2T_{\text{rms}}$. The resulting T_{eff} value is then used to calculate $a_{\max}$ and $v_{\max}$ and the response spectra.

A9 Calculation of $a_{\max}$ and $v_{\max}$

First we find the rms acceleration a_{rms} using the Parseval equation for the signal energy in the frequency and time domains:

$$a_{\text{rms}} = 2 \int_0^\infty FS^2(f) df / T_{\text{eff}} .$$

The rms velocity, v_{rms}, is found from a similar relation in which $FS(f)$ is replaced by $FS(f)/2\pi f$. We then determine the expected value of the ratio of maximum peak acceleration to its rms value (peak factor) using the following formula valid for a segment of a Gaussian process:

$$E(a_{\max}/a_{\text{rms}})^2 = 2(1 + 1/2 + 1/3 + \ldots + 1/n_p)$$
$$\approx 2[\log_e(n_p) + 0.577] ,$$

where $n_p = 2\hat{f}T_{\text{eff}}$ is the approximate number of peaks and $\hat{f}$ is the mean signal frequency determined from $FS(f)$. The Gaussian law for the amplitudes of the accelerogram assumed in SSK is only the zero approximation to reality (Gusev 1996). With a_{rms} and $a_{\max}/a_{\text{rms}}$ known, the determination of $a_{\max}$ is now straightforward; the algorithm for calculating $v_{\max}$ is similar. In a similar way we then calculate the power spectrum and the response spectrum and we estimate the macroseismic intensity from empirical correlations.